





3D Photonic integration platform based on multilayer PolyBoard and TriPleX technology for optical switching and remote sensing and ranging applications

Grant Agreement no. 780502
Research and Innovation Action (RIA)
Information & Communication Technologies (ICT)

Deliverable D6.4

Development of control unit for the 2D optical phased array beam scanning system

Lead beneficiary for the deliverable: Optagon

Contact Person: Christos Kouloumentas

Phone: +302106520711

e-mail: christos.kouloumentas@optagon-photonics.eu

Date due of deliverable: 30 September 2021 Actual submission date: 26 February 2022

Authors: Christos Kouloumentas, Panos Groumas,

Lefteris Gounaridis, Adam Raptakis

Participants: Optagon, ICCS/NTUA

Work-package: WP6
Dissemination level: Public

Nature: Demonstrator ("Accompanying report")

Version: V1.0 Total number of pages: 42

Executive Summary

The operation and the successful testing of the test PolyBoard photonic integrated circuits (PICs) with 2-dimensional (2D) optical phased arrays (OPAs) of edge emitting waveguides has been a major success of 3PEAT project because it has confirmed the possibility for 2D OPAs based on multi-layer PICs for three dimensional (3D) laser beam scanning. The operation and the testing of these OPAs was accommodated by a control electronics unit, which was developed in parallel with the modelling and the design of the OPA PolyBoard PICs, as well as in parallel with the development of the experimental testbed for the testing of the OPAs. The main evaluation equipment of this testbed is a charge-coupled device (CCD) camera for real-time acquisition of the emitted beam profile. The control electronics unit is equipped with a digital platform based on the Raspberry Pi4 micro-computer for the coordination of the OPA operation and the provision of an elegant user interface for the execution of the testing process. Coordination means in this case the control of the drivers that drive the thermal phase shifters on the PolyBoard PICs and adjust the relative phase between the antenna elements (AEs) of the OPAs, as well as the acquisition and the processing of the beam position and profile. This acquisition is made possible through the connection between the CCD camera to the digital platform of the control electronics unit.

Apart from the unit that was developed for the testing of the OPA PolyBoard PICs, a second control electronics unit was also developed for the testing of the 4×8 OPA, which is expected to be part of the final Laser Doppler Vibrometer (LDV) module of 3PEAT (Module-6). Since the operation of the OPA in this module will be based on phase shifters that will have the form of piezoelectric actuators (PZTs) in the TriPleX part of the corresponding PIC, the second unit comprises a 160-channel driver for PZTs. Each driving channel has the form of a voltage source with ultra-high output amplitude for capacitive loads in accordance with the driving needs of the PZTs that are integrated in the TriPleX platform. Finally work on the development of calibration algorithms based on the gradient descent optimization algorithm is also done and tested in order to enable the calibration of the 4×8 OPA of Module-6 without use of manual steps, which can make the entire calibration process slow and challenging.

Keywords: Photonic integration, optical phased arrays (OPAs), PolyBoard, 3D integration, beam scanning, thermal phase shifters, current sources, PZT drivers, voltage sources.

List of Acronyms

	T
2D	2-Dimensional
3D	3-Dimensional
AC	Alternating Current
AE	Antenna Element
AF	Array Factor
AWG	Arrayed Waveguide Grating
BJT	Bipolar Junction Transistor
CCD	Charge-Coupled Device
DAC	Digital to Analog Converter
DC	Direct Current
DFB	Distributed Feedback
FEP	Field Equivalence Principle
FOV	Field of View
FPGA	Field-Programmable Gate Array
GPIO	General Purpose Input Output
GUI	Graphical User Interface
IEEE	Institute of Electrical and Electronic Engineers
I2C	Inter-Integrated Circuit
IC	Integrated Circuit
IR	Infra-Red
LDV	Laser Doppler Vibrometer
МО	Microscope Objective
ММІ	Multi-Mode Interference
MZI	Mach-Zehnder Interferometer
NA	Numerical Aperture

NIR	Near Infra-Red
ОРА	Optical Phased Array
OSA	Optical Society of America
PC	Polarization Controller
РСВ	Printed Circuit Board
PCT	Patent Cooperation Treaty
PIC	Photonic Integrated Circuit
PZT	Lead zirconate titanate (Piezoelectric element)
RIE	Reactive Ion Etching
RPi4	Raspberry Pi4
Si	Silicon
SPI	Serial Peripheral Interface
TE	Transverse Electric
TM	Transverse Magnetic
USB	Universal Serial Bus
UV	Ultra-Violet

Table of Contents

Executive Summary	2
List of Acronyms	3
Introduction	6
1. 3PEAT OPA concept and development of OPA PICs	7
1.1 Fundamentals of optical phased arrays	7
1.2 The 3PEAT concept for the development of 2D OPAs	8
1.3 Modelling and simulation results	10
1.4 Development of OPA PolyBoard PICs	18
2. Development of control electronics and testing of PolyBoard OPA PICs	19
2.1 Design and development of control electronics	20
2.2 Basic characterization results of the PolyBoard OPA PICs	24
3. Development of control electronics for the final OPA PICs of 3PEAT project	31
3.1 Design of final OPA PICs of 3PEAT project	31
3.2 Development of control electronics	32
3.3 Development of calibration process and algorithms	35
Conclusions	36
Statement on exploitation potential and activities	36
References	37
List of Figures	39

Introduction

The present document reports on the control electronics that have been developed by Optagon in collaboration with partners ICCS, FhG-HHI and LioniX in order to support the operation of the optical phased arrays (OPAs) of 3PEAT for the execution of laser beam scanning in photonics-based modules for Laser Doppler Vibrometer (LDV) applications.

The original plan of 3PEAT for the OPAs of the project was the development of 2dimensional (2D) OPAs on hybrid photonic integrated circuits (PICs) consisting of a PolyBoard part with multiple waveguiding layers, and a silicon nitride (TriPleX) part with a single waveguiding layer. The integration of the two parts in the form of a single hybrid PIC can be based either on a 2D butt-end coupling method or on a 3D coupling method using the evanescent field of the waveguided light. Within these hybrid PICs, the edge emitting waveguides at the various waveguiding layers of the PolyBoard part can serve as antenna elements (AEs) that form a 2D array with horizontal rows and vertical columns. Moreover, within the same PICs, the piezoelectric actuators (PZTs) in the TriPleX part can serve as the phase shifting elements that will control the relative phase of the AEs, and will select the propagation direction of the emitted laser beam. Although a version of these OPAs is still under development as part of 3PEAT Module-6 and is expected to be made available for tests after the official end date of the project (January 31, 2022), the actual validation of the 3PEAT OPA concept was realized using precursor structures in the form of monolithic PolyBoards with two waveguiding layers and 8 edge emitting waveguides forming a 2×4 OPA each. In these PICs, the phase shifters for the control of the relative phase of the AEs were based on heating electrodes (thermal phase shifters) on the PolyBoard platform.

With this background, the content of the present document has been organized in four separate sections. In section 1, we present the main OPA concept of 3PEAT, we summarize the simulation results that have been produced in collaboration with ICCS for the modelling of the OPA operation, for the design of the OPA PICs and for the development of the control electronics, and we present the OPA PICs that were developed by FhG-HHI. In section 2, we present the architecture of the control electronics (digital and analog part), and we report on the specific version of these electronics that was developed for the operation of the PolyBoard PICs in collaboration with ICCS. The contribution of ICCS had to do with the development of the interface between the control electronics with the infra-red (IR) camera of the institute for the tracking of the scanning process, and with the provision of guidelines for the development of the user interface. Moreover, within the same section we report on the experimental results that were successfully obtained and confirmed the validity of the main OPA concept of 3PEAT. In section 3, we continue and present the version of the control electronics that has been prepared for the operation of the hybrid PIC comprising PZT-based phase shifters in the TriPleX part of the PIC instead of thermal phase shifters in the

PolyBoard part of the hybrid PIC for the adjustment of the relative phase between the AEs (edge emitting waveguides). This version is ready, and will be used for the operation of the OPA of Module-6 as soon as this will be made available for testing at ICCS lab. In section 4, we make a high-level presentation of the algorithm that has been developed for the calibration of the OPA. This algorithm was not necessary for the operation of the OPAs on the precursor PolyBoards due to their small size (2×4 array), but it is expected to be necessary for the operation of the OPA in Module-6 due to its significantly larger size (4×16 array) and complexity. Finally in the last section (conclusions), we conclude, and describe future work as part of Optagon plan for the exploitation of our participation in 3PEAT.

1. 3PEAT OPA concept and development of OPA PICs

The material that is reported in the present section of the document has been presented to a large extent in the scientific publication (IEEE/OSA Journal of Lightwave Technology) that was achieved by Optagon, ICCS and FhG-HHI as part of the dissemination and exploitation plan of 3PEAT project [1].

1.1 Fundamentals of optical phased arrays

OPAs have the possibility to replace the moving mirrors and lenses in the laser beam scanning unit of optical sensing and free-space communication modules, enabling realizations of that unit in a compact, robust and low-cost form [2-6]. Typical implementations of OPAs in the form of PICs bring together a set of light outcoupling structures that act as AEs, a set of phase shifters that control the phase relations between the AEs, and a set of optical couplers that split the input laser light between the AEs of the OPA. The far-field of each OPA emerges as the coherent addition of the emitted fields that correspond to the individual AEs. Provided that the spatial arrangement and the phase relations of these AEs are suitable, this far-field can exhibit a main radiation lobe that points to a well-defined and well-controlled direction.

The grating couplers and the edge-emitting waveguides at the end facet of the PICs have been hitherto the two most common types of optical AEs in OPA implementations [7]. In the case of the edge-emitting waveguides, which is to our interest in 3PEAT project, the propagating light finds its way out of the waveguides at the end-facet of the PIC, and is emitted into the air. Compared to the grating couplers, the edge-emitting waveguides have significant advantages when used in linear arrays for scanning on a single plane: their radiation efficiency is unity, their radiation pattern is smooth and fully defined by the profile of the waveguided mode, and their size as AEs is the smallest possible one, enabling OPA realizations with large number of AEs and small inter-element spacing (pitch). The main drawback of the end-fire waveguides on the other hand is the fact that they cannot form 2D arrays in planar PICs to support a 2D scanning operation, which is typically required in

most applications. To overcome this drawback, efforts have been made to develop 3D silica (glass) structures with waveguides at multiple layers that can facilitate 2D OPAs with end-fire waveguides [8-9]. Despite the innovation of these works, there are two critical drawbacks of the silica as material system for the implementation of such a concept. The first one is the need for hybrid integration of the silica structure with a PIC that can host the optical couplers and the phase shifters of the OPA. The second one is the weak mode confinement in the silica waveguides that leads to strong optical coupling between the waveguides when they get in proximity. As a result, the OPA has to be designed with a large vertical and lateral pitch (>15 nm), which leads to small range of steering angles (<5°) [9]. This range is defined in fact as the angular spacing between the main lobe and the grating lobes in the radiation pattern of the OPA.

1.2 The 3PEAT concept for the development of 2D OPAs

3PEAT has been conceived among others upon the perception that PolyBoard can be an ideal photonic platform for the development of 2D OPAs with edge-emitting waveguides. PolyBoard is a general-purpose polymer platform that supports the monolithic integration of various structures and can act as motherboard for the hybrid integration of heterogeneous elements [10]. The fabrication of PolyBoard PICs involves simple steps, which can be repeated in order to develop 3D PICs with multiple waveguiding layers and vertical couplers for light transition between these layers [11]. Within 3PEAT these possibilities are used for the first time as a practical means to develop 3D PolyBoard PICs that will realize 2D OPAs with edge-emitting waveguides for 2D laser beam scanning units.

In more detail, PolyBoard is a single-mode photonic integration platform based on optical polymers (n_{core} = 1.48, n_{clad} = 1.45) that offers low propagation loss at 1550 nm (0.7 dB/cm) and possibility for fabrication of multi-functional PICs. This possibility is based on the monolithic integration of elements such as multi-mode interference (MMI) couplers, Mach-Zehnder interferometers (MZIs), arrayed waveguide gratings (AWGs), attenuators, optical hybrids and thermal phase shifters, on the hybrid integration of indium phosphide elements such as gain sections, modulators and photodiodes, and on the assembly of thin films and micro-optical elements inside slots and grooves on the surface of the polymer platform [10]. The cross-section of the single-mode waveguide for operation at 1550 nm is 3.2 μ m × 3.2 μ m in size. Due to the symmetry of this cross-section, the supported mode is hybrid with a transverse electric (TE) and a transverse magnetic (TM) component. The presence and strength of these components in the propagating field depend on the excitation conditions of the waveguide on each occasion.

As already described in previous 3PEAT reports and deliverables, the fabrication of the standard PolyBoard PICs with a single waveguiding layer is based on the use of two polymer resins (waveguide and cladding resin) and successive layer deposition steps. These steps

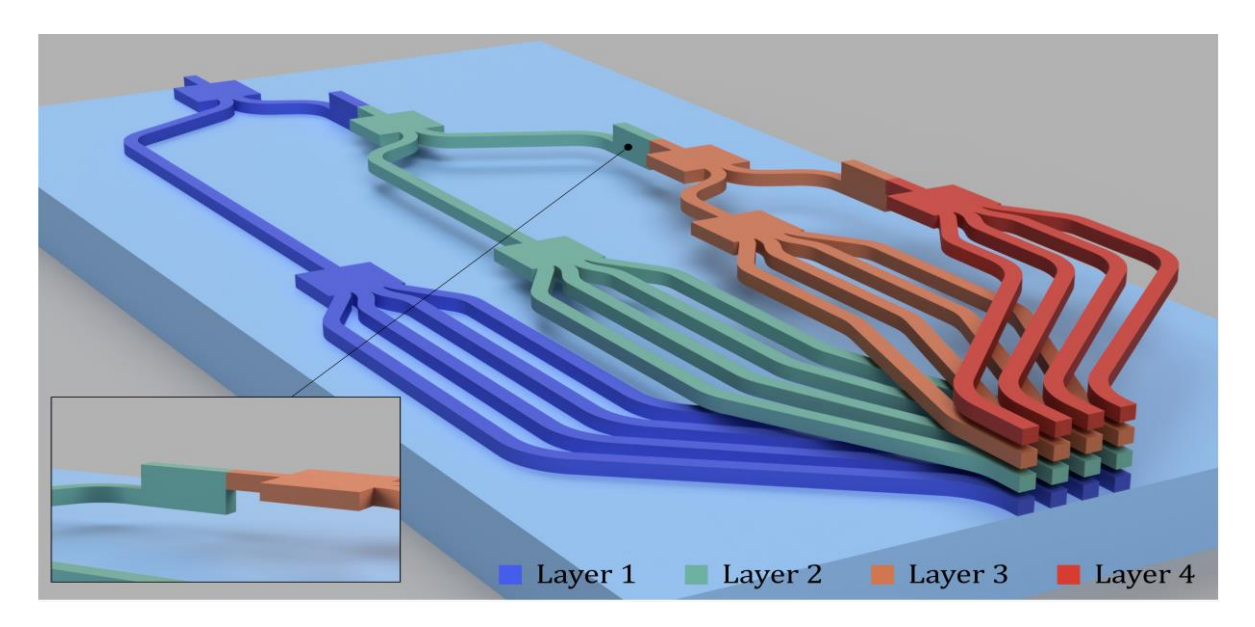


Figure 1: Fundamental 3PEAT concept for the development of 2D OPAs based on PolyBoard PICs with multiple waveguiding layers and vertical MMI couplers for light coupling between the adjacent waveguiding layers. Edge emitting single-mode waveguides serve as AEs at the end-facet of each PIC. The cladding material is omitted in the representation for clarity. A 4×4 OPA is shown as example. Any layer can be used as seed layer. Vertical couplers that couple directly the input light to the target layer without involving the intermediate ones can be alternatively used. Inset: Close view of a vertical MMI coupler followed by a lateral one.

involve the spin-coating of the cladding resin on a silicon (Si) substrate, the spin-coating of the waveguide resin, the structuring of the waveguiding layer using ultra-violet (UV)-lithography and reactive ion etching (RIE), and the spin-coating of a second layer of cladding resin to form the top cladding layer. This process can be repeated many times with different mask sets resulting in PolyBoard PICs with multiple waveguiding layers.

Within this 3D structure, each layer can be independently formed in a way that retains its potential to support the full set of functionalities offered by PolyBoard technology. Furthermore, the flexibility to use intermediate deposition steps enables the structuring of vertical MMI couplers that can couple the light between adjacent layers [11]. With this integration technology, it is thus possible to develop PolyBoard PICs with lateral MMI couplers, vertical MMI couplers and thermal phase shifters that receive an optical input and distribute this input among a number of output waveguides with precise phase control. Since the waveguides can run at different layers, it is possible to develop a 2D array of edge-emitting waveguides at the end-facet of a 3D PolyBoard PIC, supporting the scanning of an optical beam on both the azimuthal and the elevation plane. The pitch of the array in the horizontal axis is determined by the pitch of the edge-emitting waveguides at the same waveguiding layer, whereas the pitch in the vertical axis is determined by the spacing between the waveguiding layers in the 3D structure of the PIC. Figure 1 shows the concept of the 2D OPAs based on a 3D PolyBoard PIC taking as example the case of a 4×4 OPA.

1.3 Modelling and simulation results

A concrete investigation of the radiation performance of the OPAs in the PolyBoard platform preceded the design of the OPA PICs and the development of the control electronics. The investigation started from the modelling of the edge-emitting waveguide as the basic AE of the OPAs, and continued with the extraction of the radiation features of each OPA in the far-field from the combination of the radiation features of the basic AE with the array factor (AF) that corresponds to each OPA. In more detail:

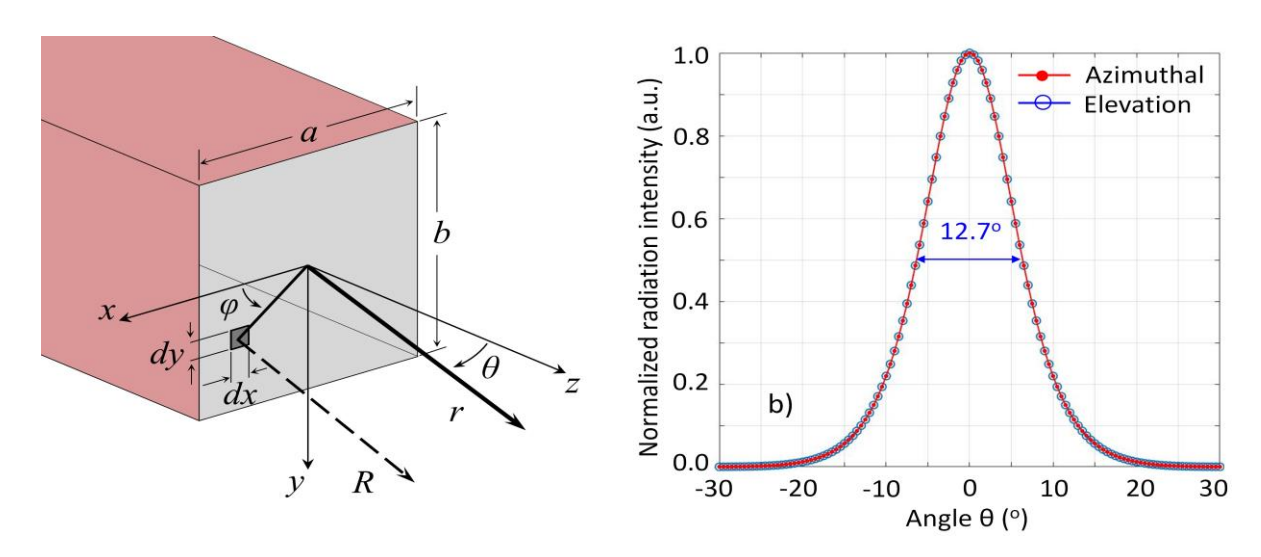


Figure 2: a) Coordinate system and geometry for the modelling of the edge-emitting PolyBoard waveguide as an aperture antenna using the Field Equivalence Principle (FEP), and b) Normalized radiation intensity of the edge-emitting PolyBoard waveguide on the azimuthal and the elevation plane.

An edge-emitting PolyBoard waveguide constitutes a rectangular aperture antenna. The field radiated to the air at the end-facet of the waveguide can be calculated at every point of the hemisphere outside the PolyBoard PIC using the Field Equivalence Principle (FEP). The theory and the application steps of the FEP is described in detail in various textbooks [12]. Its use involves four steps. In the first one, an imaginary surface that encloses the actual radiation source is defined. In the second step, the actual radiation source is replaced by fictitious sources that reside on the defined surface and yield the same field as the actual source within the volume of interest, which is in fact the volume outside the surface. In the third step, these equivalent sources are calculated using the boundary conditions on the imaginary surface. In order to make this calculation, one has to use the information about the actual value of the electromagnetic field on the surface, and to additionally assume that the corresponding field in the volume that is enclosed by the surface is zero. Finally, in the last step, the equivalent sources that have been calculated in the previous step are used for the calculation of the vector potentials and the electromagnetic field in the volume outside the surface. In the case of an edge-emitting PolyBoard waveguide with the geometry shown

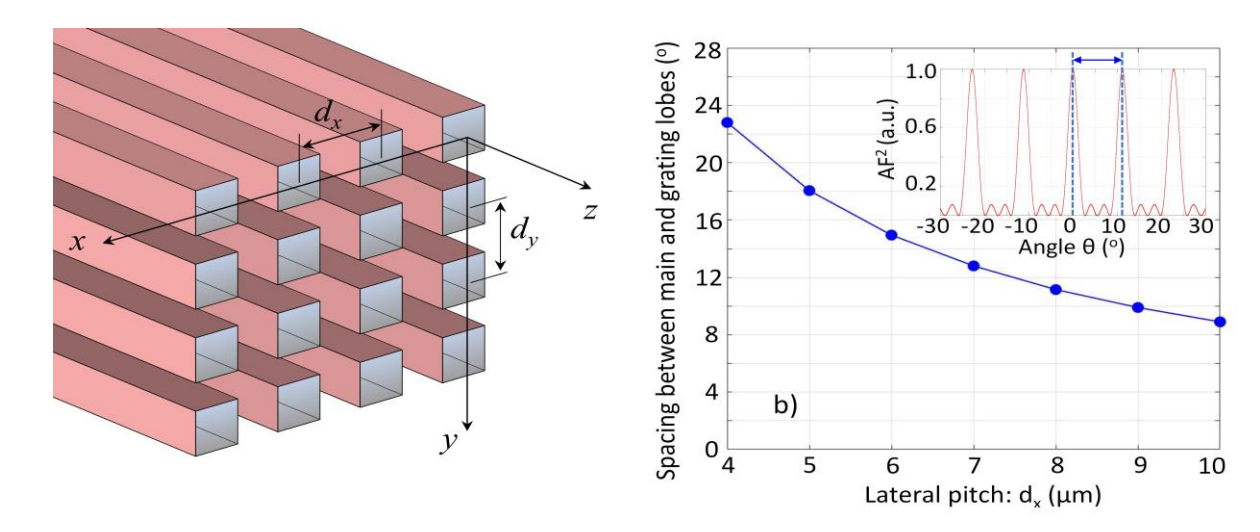


Figure 3: a) Coordinate system and geometry for the modelling of OPAs with edge-emitting waveguides in PolyBoard PICs, and b) Angular spacing between the main and the grating lobes of the AF (squared) in a linear OPA as a function of the pitch. Results are not PolyBoard specific. Inset: Example AF (squared) corresponding to a linear OPA with 4 AEs, 8 µm pitch and 0° steering angle.

in Figure 2a, it is convenient to consider the plane at the end-facet of the waveguide as an imaginary surface that extends to the infinity and encloses the radiation source. With this choice, the information about the mode profile inside the waveguide can be used to determine the actual field on the imaginary surface, and eventually to calculate the far-field radiation of the waveguide. The radiation patterns that emerge in the two cases are identical, and have a single lobe. With reference to the spherical coordinate system and the geometry of Figure 2a, this common pattern has its maximum at $\theta=0$, and is symmetric around the z-axis without any dependence on the angle φ . Figure 2b provides an insight into the radiation intensity $U_o(r_o, \theta, \varphi)$ of this pattern at a random radius r_o in the far-field. The first curve with red dots in this diagram refers to the azimuthal plane and presents the radiation intensity as a function of θ for $\varphi = 0^o$ (positive θ -axis) and $\varphi = 180^o$ (negative θ -axis). The second curve with blue empty circles refers to the elevation plane. It has a perfect overlap with the first one and presents the dependence of the radiation intensity on θ for $\varphi = 90^o$ (positive θ -axis) and $\varphi = 270^o$ (negative θ -axis). It is noted that in reality, the angle θ takes only positive values. However, in the diagram of Figure 2a, we use both the positive and the negative part of the axis to discriminate between the θ values that correspond to $\varphi = 90^{\circ}$ and those that correspond to $\varphi = 270^{\circ}$ or between the θ values that correspond to $\varphi=0$ and those that correspond to $\varphi=180^o$. On both planes, the Full-Width at Half-Maximum (FWHM) of the radiation intensity is approximately 12.7°. Since the radiation pattern is symmetric around the z-axis, the FWHM remains the same for any angles φ and $\varphi + 180^{\circ}$, and describes unambiguously the directivity of the PolyBoard edge-emitting waveguide as an optical antenna.

In PolyBoard PICs with a single waveguiding layer, the edge-emitting waveguides act as a set of identical AEs that form a linear OPA. In the case of uniform OPAs, the pitch is constant, the excitation fields have the same magnitude, and the differential phase β_x in the excitation of each AE compared to its preceding one remains the same for all AEs. With reference to the definition of the axes in Figure 3a, the array factor (AF) of a uniform OPA is expressed as per the relation:

$$AF(\theta,\varphi) = \sum_{n=1}^{N} e^{i \cdot (n-1) \cdot (k \cdot d_{x} \cdot \sin\theta \cos\varphi + \beta_{x})}$$
(1)

where N the number of antenna elements, d_x the pitch of the linear array and k the wavenumber in the free-space. The direction of the main lobe of the AF on the azimuthal plane is controlled by the parameter β_x . Since however the pitch of the PolyBoard OPAs is much larger than the half of the wavelength at 1550 nm, grating lobes are also present in the AF, setting limitations on the maximum steering angle and the field-of-view (FOV) that are offered by the OPAs. The inset of Figure 3b presents as an example the main and the grating lobes of the square of the AF that corresponds to a 4-element linear OPA at 1550 nm with 8 μ m pitch and with 0° steering angle on the azimuthal plane. The main diagram of Figure 3b presents on the other hand the angular spacing between the main and the grating lobes of the square of the AF as a function of the pitch. Although the dependence shown in this diagram is general and holds true for all uniform OPAs, it is of particular value for the design of PolyBoard OPAs, since the latter are based on waveguides that are rather wide (3.2 μ m) and offer weak mode confinement due to their low refractive index contrast. Using the radiation intensity (U_0) of the PolyBoard edge-emitting waveguide and the AF of a linear OPA, the radiation intensity (U) of a single-layer PolyBoard OPA is calculated as follows:

$$U(r,\theta,\varphi) = U_o(r,\theta,\varphi) \cdot [AF(\theta,\varphi)]^2$$
(2)

Figure 4a presents two example cases for the radiation intensity of such an OPA on the azimuthal plane. The first one is shown with red solid line and corresponds to an OPA with 4 AEs, 8 µm pitch and steering direction at 4°. The second one is shown with blue dotted line and corresponds to an OPA with 8 AEs, 6 µm pitch and direction at -4°. The radiation intensity of the basic AE is also illustrated as an envelope in agreement with the physical meaning of Eq. (2). In both cases, only one grating lobe is clearly observed due to the suppression imposed on all other ones. The angular spacing between each main lobe and its companion grating lobe is primarily defined by the pitch of the respective OPA. It is noted however that this spacing is slightly smaller than the corresponding spacing in Figure 3b between the lobes of the AF2. This reduction is a result of the multiplication between the

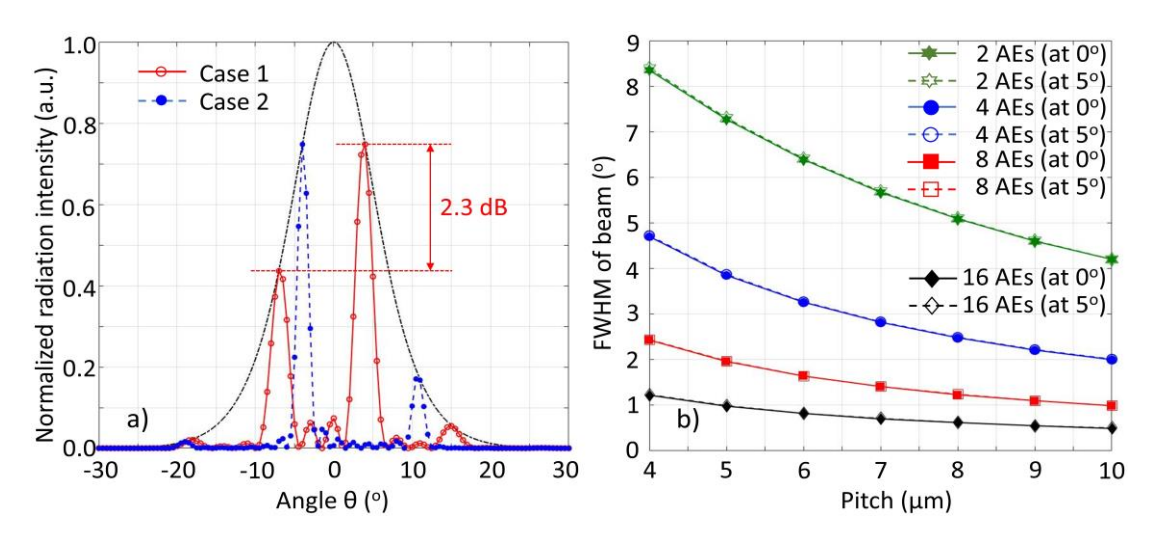


Figure 4: a) Exemplary radiation intensity of two linear PolyBoard OPAs on the azimuthal plane: The first one (Case 1) has 4 AEs, 8 μ m pitch and direction at +4°, and the second one (Case 2) has 8 AEs, 6 μ m pitch and direction at -4°. b) FWHM of the main lobe of the radiation intensity as a function of the pitch for different number of AEs and steering angles.

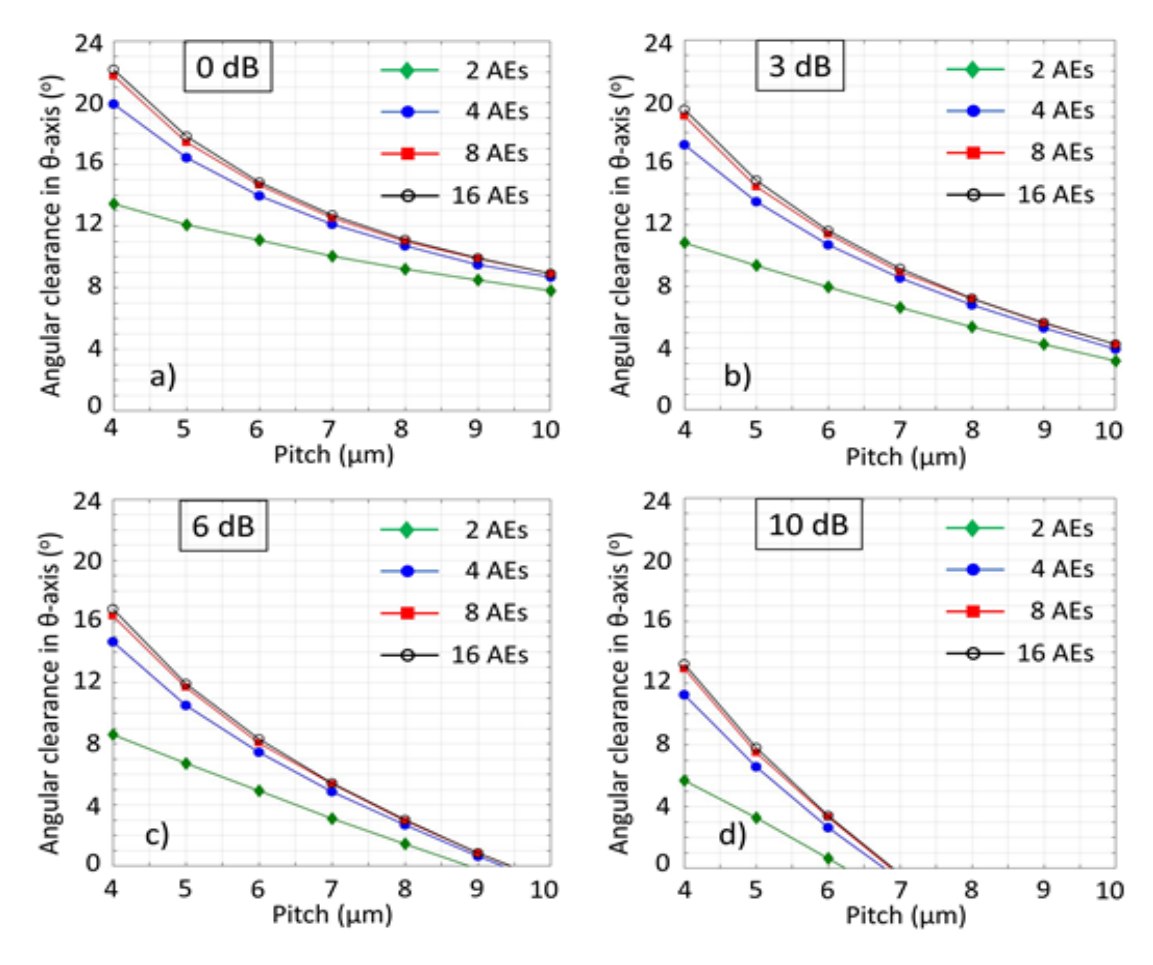


Figure 5: Radiation intensity of linear PolyBoard OPAs on the azimuthal plane: Angular clearance, wherein the main lobe of the radiation pattern is higher than any grating lobe by: a) 0 dB, b) 3 dB, c) 6 dB, and d) 10 dB.

AF² and the radiation intensity of the basic AE, and is present for any pitch or number of AEs. Finally, Figure 4b presents simulation results regarding the beam width in the radiation pattern of a PolyBoard OPA. It reveals the strong dependence of the FWHM of the main lobe on the number of AEs, and the weaker dependence on the waveguide pitch. On the other hand, no dependence on the steering angle can be observed for angles that remain within the range of interest. Looking carefully at the main and the grating lobe in the first case of Figure 4a, we find that their relative intensity ratio is 2.3 dB. If the beam is steered further to the right with θ larger than 4° , this ratio drops. If on the contrary, the beam is pulled to the other direction, the ratio increases and gets back to its initial value when the main lobe is at -4°. The angular space from -4° to 4° represents in this example the symmetric clearance around 0°, wherein the main lobe is larger than any grating lobe by at least 2.3 dB. Figure 5a-d extend this investigation and present the clearance around 0°, wherein the main lobe of the radiation pattern remains larger than any grating lobe by at least 0, 3, 6 or 10 dB, respectively. By default, the 0 dB clearance shown in Figure 5a reveals the spacing between the main and the grating lobes for the respective number of AEs and waveguide pitch. On the other hand, the 3 dB, 6 dB and 10 dB clearance can serve as a practical metric for the assessment of the FOV that can be achieved, depending on the grating lobe suppression requirements of each application.

In PolyBoards with multiple waveguiding layers, the end-fire waveguides form a plane (2D) OPA. The radiation properties presented in the previous paragraph for the azimuthal plane in the case of linear OPA can be extended without modification to the elevation plane to describe the radiation pattern of a plane OPA and the possibility for 2D scanning of that pattern on the azimuthal and the elevation plane. Using again the spherical coordinate system and the definition of the axes in Figure 2a and Figure 3a the AF of a uniform plane OPA is given as:

$$AF(\theta,\varphi) = \sum_{n=1}^{N} \sum_{m=1}^{M} e^{i \cdot (n-1) \cdot (k \cdot d_x \cdot \sin\theta \cos\varphi + \beta_x)} e^{i \cdot (m-1) \cdot (k \cdot d_y \cdot \sin\theta \sin\varphi + \beta_y)}$$
(3)

where N, d_x and β_x the number of AEs, their pitch and their differential phase along the x-axis, while M, d_y and β_y the number of AEs, their pitch and their differential phase along the y-axis. The scanning process on the azimuthal plane is controlled by the differential phase β_x , whereas the scanning process on the elevation plane is controlled by the differential plane β_y . The total radiation intensity (U) is given again by Eq. (2), using the radiation intensity (U_o) of the end-fire waveguide and the AF of the plane OPA from Eq. (3).

A significant part of the simulation studies had to do with the investigation of the optical cross-talk between the PolyBoard waveguides aiming to reduce this cross-talk without

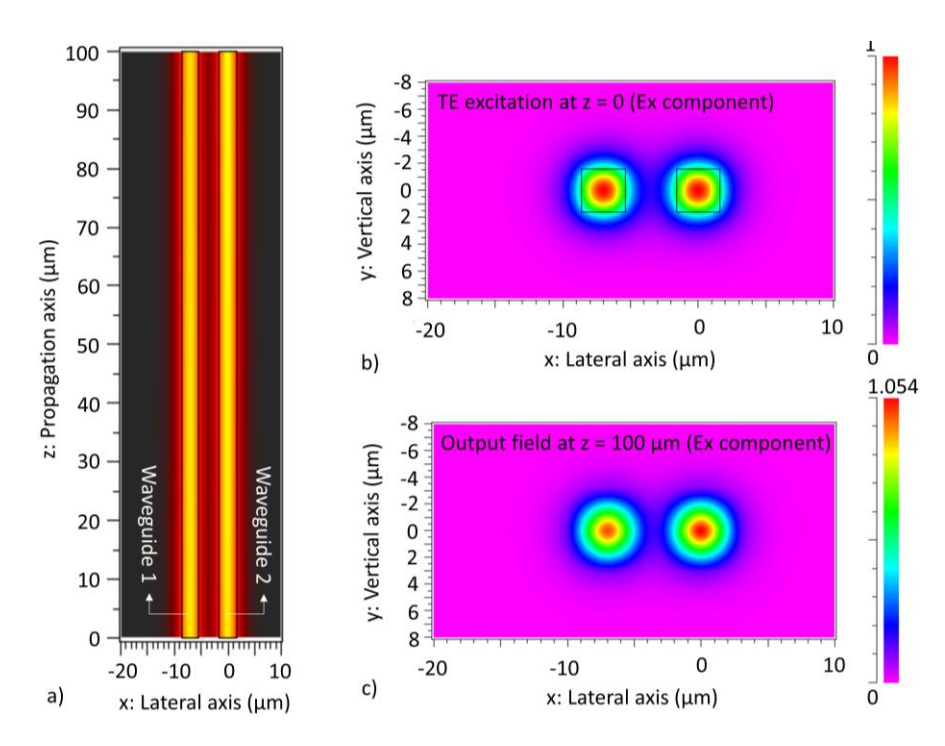


Figure 6: Simulation study for the estimation of the crosstalk between two PolyBoard waveguides: a) Pattern for 100 μ m propagation, b) TE excitation of the two waveguides, and c) Output fields with dominant Ex component at z = 100 μ m. The three diagrams correspond to 7 μ m waveguide pitch, -30° phase in the excitation of waveguide 1, and 0° phase in the excitation of waveguide 2.

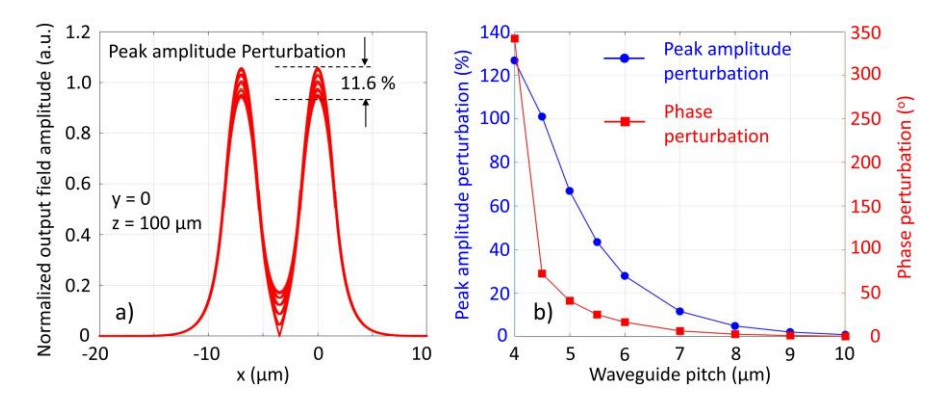


Figure 7: a) Amplitude perturbation in the output field of waveguide 2 ($z = 100 \mu m$) due to the phase variation in the excitation of waveguide 1 (see Figure 6a). The 12 curves correspond to excitation phase from -180° to +150° with 30° step. b) Main results: Amplitude and phase perturbation at waveguide 2 output as a function of the pitch. The values are for the center of waveguide 2 (x = 0, y = 0).

increasing unnecessarily the pitch between the AEs of the OPAs. In more detail, the results in Figure 4 and Figure 5 for the linear OPAs in single-layer PolyBoards, and the extension of these results to the case of the plane OPAs in multi-layer PolyBoards are based on the assumption that the phase of each AE can be independently controlled. This holds true, when the pitch of the OPAs is large enough, but it is not true when the waveguides are brought in proximity and start getting coupled. Within this context, parts of the diagrams in

Figure 4b and Figure 5 may not be of any practical value since they might correspond to waveguide spacings that do not prevent this kind of detrimental coupling. To evaluate the strength of the waveguide coupling as a function of the pitch, and define a conventional cut-off pitch as a guideline for the design of OPAs in single- and multi-layer PolyBoards, we took the simplest case of two parallel PolyBoard waveguides with 100 µm length (see Figure 6a), and we simulated the light propagation in those waveguides. Both waveguides were excited by their fundamental eigenmode with TE polarization and peak amplitude normalized to unity. In all simulations for a particular pitch, the phase of the excitation field in the right-most waveguide (denoted as waveguide 2) was zero, whereas the phase of the excitation field in the left-most waveguide (denoted as waveguide 1) varied from -180° to +180°. Figure 6 presents as example a case that corresponds to 7 μm pitch and -30° phase of the excitation field at the input of waveguide 1. More specifically, Figure 6a illustrates the propagation pattern and reveals in a qualitative way the optical crosstalk between the two waveguides. Figure 6b presents in turn the cross-section of the two waveguides and the distribution of the TE fields that were employed for the excitation of the two waveguides at z = 0. Finally, Figure 6c depicts the corresponding distribution of the output fields at z = 100 μm, and makes evident the asymmetry that is induced between the two waveguides due to the optical crosstalk. The perturbation of the amplitude and the phase of the output field of waveguide 2 with respect to the corresponding amplitude and phase of the output field, when this waveguide is alone, depends both on the pitch and on the phase of the excitation field at the input of waveguide 1. The level of this perturbation at the center of the cross-section of waveguide 2 can be used as a good metric for the assessment of the coupling between the two waveguides. Along the same line, Figure 7a presents as an example the peak amplitude perturbation of the output fields, when the pitch is 7 µm and the excitation phase at the input of waveguide 1 varies from -180° to +150° with 30° step (i.e. 12 curves in total). The perturbation is the same for both waveguides with a range of almost 11.6% of the peak amplitude at the input. The range of the phase perturbation is not shown in this diagram, but it is 6.6° in absolute terms. Figure 7b summarizes the ranges of the amplitude and phase perturbation as a function of the waveguide pitch for values between 4 and 10 µm. As shown, for pitch equal or larger than 8 μm, the perturbation is negligible, and the waveguides remain practically decoupled. For pitch between 8 and 6 µm, the perturbations start rising, but remain moderate and manageable, whereas for pitch below 6 µm, the rise becomes much more abrupt. Based on these observations, the conclusion of our modelling and simulation studies was that the value of 6 µm can be a safe limit for the pitch of uniform OPAs in the PolyBoard platform. In order to further investigate the impact of the optical crosstalk on the radiation pattern of a PolyBoard OPA, we extended our previous study, and we investigated the far-field radiation pattern of the two waveguides as a function of their spacing, when the relative

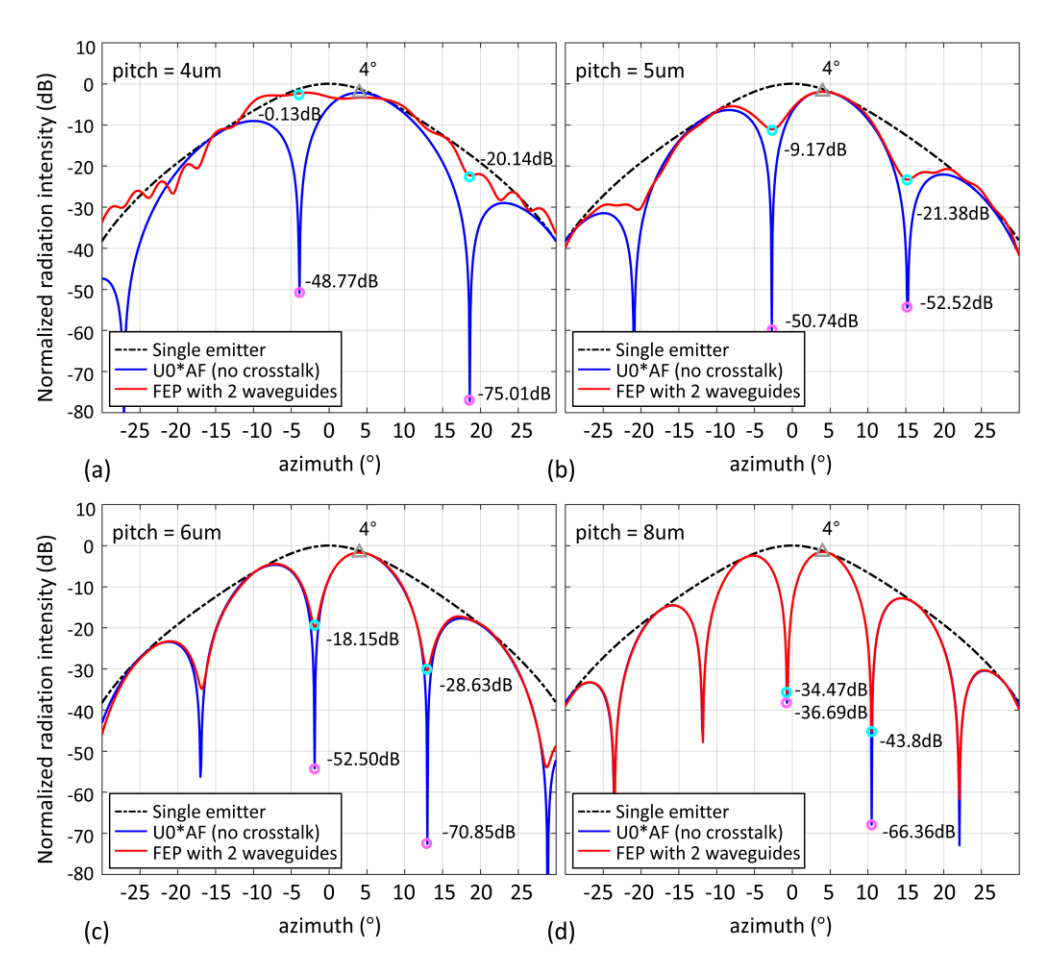


Figure 8: Far-field radiation intensity of two edge-emitting PolyBoard waveguides with relative phases that lead to beam steering at 4° on the azimuthal plane. The diagrams correspond to waveguide spacing equal to: a) $4 \, \mu m$, b) $5 \, \mu m$, c) $6 \, \mu m$, and d) $8 \, \mu m$. The two curves in each diagram correspond to different simulation methods. The method of the blue solid curve does not take into account the optical crosstalk between the two waveguides, whereas the method of the red-dashed curve does. The difference between the two curves reveals the impact of the crosstalk on the radiation pattern for the respective waveguide spacing.

phases of the two waveguides were adequately adjusted for steering of the main lobe at 4° . For each spacing, the investigation was based on the comparison between the radiation patterns that are obtained with two different simulation methods. The first one is the method presented above, involving the calculation of the radiation intensity (U_o) of the basic AE with the help of the Field Equivalence Principle (FEP), the calculation of the AF that corresponds to the two AEs for their specific spacing, and the combination of the two quantities with the help of Eq. (2). It is clear that this method does not take into account the optical crosstalk during the co-propagation of the optical waves along the two waveguides. The second method treats the combination of the two waveguides as a single AE. It uses the electro-magnetic field at the end-facet of the two waveguides as the input for the implementation of the FEP and the direct calculation of the radiation intensity of the two waveguides in the far-field. Since the electromagnetic field that serves as input is the

result of the co-propagation of the optical waves inside the two waveguides, this second method takes clearly into account the optical crosstalk. Any difference between the results from the two methods can thus be attributed to the impact of this crosstalk. The diagrams in Figure 8 present in logarithmic scale the normalized radiation intensity obtained with the two methods for spacing equal to 4, 5, 6 and 8 μm, respectively. The point of minimum intensity between the main and the grating lobe is the most indicative one for the comparison of the two curves in each diagram. As observed, the two methods give practically the same result in the case of 8 µm spacing. The difference remains small in the case of 6 µm spacing, whereas it gets substantially larger in the case of 5 and 4 µm spacing, revealing the strong impact of the crosstalk on the radiation pattern in these cases. Finally, it is also noted that as already described, the perfect symmetry of the cross-section of the single-mode waveguide in the PolyBoard platform leads to the creation of exactly the same radiation pattern from an OPA, both when the excitation of the AEs is done with the TE mode and when is done with the TM mode of the PolyBoard waveguides. A small polarization sensitivity of the OPAs in the PolyBoard platform can still be expected however due to the polarization sensitivity of on-chip components other than the waveguides such as the optical (MMI) couplers.

1.4 Development of OPA PolyBoard PICs

The simulation results that have been presented in the previous paragraph were used for the design of the PolyBoard PICs that provided the experimental proof-of-concept regarding the potential of the PolyBoard platform for laser beam scanning. Two types of PolyBoard PICs were developed. The first one corresponds to single-layer PICs with linear 1×4 OPAs. Three versions of these PICs were designed with lateral pitch equal to 6, 8 and 10 μ m to experimentally investigate the impact of the pitch on the beam parameters and the beam scanning performance. The second type corresponds to PICs with two waveguiding layers that support the development of 2×4 OPAs. Three versions of these PICs were designed with lateral pitch equal to 6, 8 and 10 μm, respectively. The vertical pitch was 7.2 μm in all versions. Figure 9 presents the mask layout and a micro-photograph of the version with 10 μm lateral pitch. On the left side of the circuit the input signal is split in two parts by a lateral 1:2 MMI coupler. The light at the second output of this coupler is transferred to the upper waveguiding layer by means of a vertical MMI coupler with 1350 μm length and 10.4 μm height. At each layer the light is split in four equal parts by a lateral 1:4 MMI coupler and the optical phase inside the output waveguides is adjusted by thermal phase shifters. The four waveguides are brought in proximity by means of S-bends, and run in parallel till the end-facet of the PIC in order to get emitted by the edge-emitting waveguides (AEs). It is noted that the linear 1×4 OPAs at the two layers are laterally aligned to each other as much as possible so as to form a rectangular 2×4 OPA (see Figure 9c). The fabrication of the single-

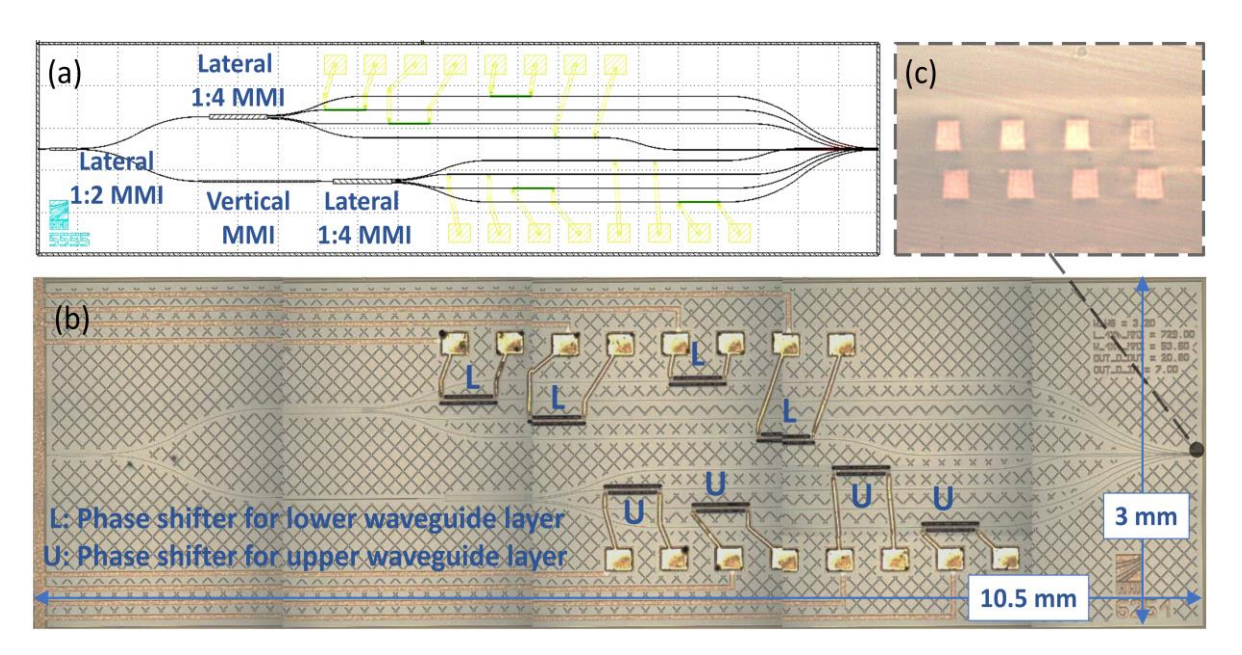


Figure 9: a) Mask layout for the fabrication of 2×4 OPAs with 10 μ m lateral and 7.2 vertical pitch in 2-layer PolyBoards, and b) Photograph of a respective PolyBoard PIC (top-view). The tags (L or U) next to each heating electrode indicate, whether the particular electrode is used for the control of a waveguide at the lower or the upper layer of the 2-layer PolyBoard PIC. c) Micro-photograph of the end-facet of the same PIC, where the edge-emitting waveguides that act as the optical AEs of the OPA are clearly visible.

layer PICs was based on the standard steps of PolyBoard technology. The fabrication of the 2-layer PICs on the other hand was realized using the repetitive steps of 3D PolyBoard technology. It is noted that in the case of the 2-layer PICs, all heating electrodes were fabricated on the top of the PICs, and for this reason they are visible in the same way under the microscope (see Figure 9b). The fact that the heating electrodes were fabricated on the top implies that the four electrodes that control the waveguides of the upper layer are closer to their companion waveguides, whereas the four electrodes that control the waveguides of the lower layer are further apart. As a consequence, the operation of the first quartet is more energy efficient having the same current requirements for pi-phase shift as the electrodes in the single-layer PICs (approximately 16 mA). On the other hand, the required current for pi-phase shift in the electrodes of the second quartet is approximately 20 mA. After the end of the wafer processing, all PolyBoard PICs were diced, and taken further for characterization at the PIC level. The best performing ones were shipped to the lab of ICCS for system testing using the control electronics of Optagon.

2. Development of control electronics and testing of PolyBoard OPA PICs

The present section presents the design and the development of the control electronics unit for the operation of the PolyBoard OPA PICs, and the results that were obtained at the lab of ICCS from the characterization of these PICs with the help of the control electronics.

2.1 Design and development of control electronics

The design of the electronics for the operation control of the PolyBoard OPA PICs had as an objective the development of a unit that can control independently the phase shifters of the OPAs and apply the necessary currents to each one of them in order to achieve the target phase relations between the AEs, and the target direction for the emitted beam. It also had as a second objective the development of a communication link between the main controller of the unit and the infra-red (IR) camera for the acquisition of the beam profile and the application of certain processing functionalities (such as averaging and fitting) on these profiles. The main parts of the control electronics unit in this case comprised three basic elements: A Raspberry Pi micro-computer as the smart digital controller of the unit, a Texas Instrument digital-to-analog converter (DAC) for the provision of precise voltage signals, and an array of custom made voltage-controlled circuits acting as current sources for the operation of the heating electrodes (thermal shifters) on the PolyBoard platform. In more detail, the main constituent components of the control electronics unit have been:

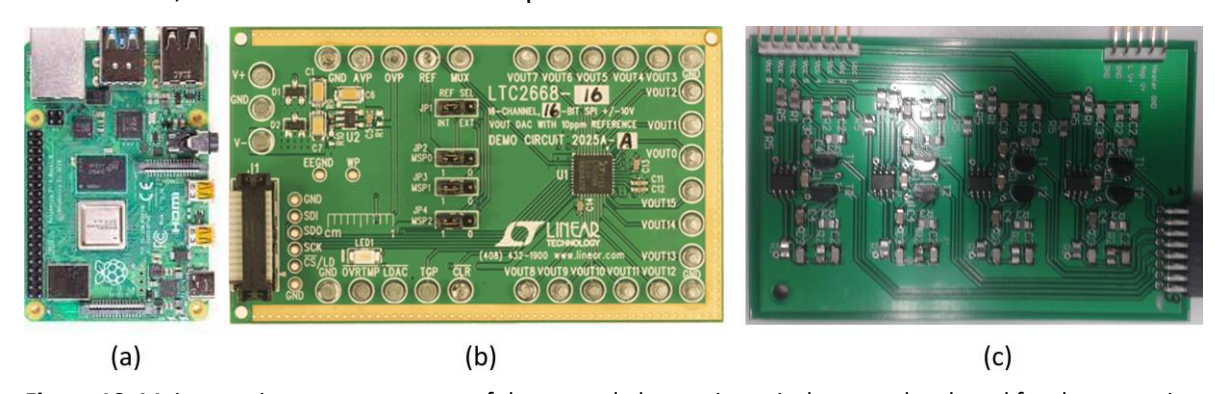


Figure 10: Main constituent components of the control electronics unit that was developed for the operation of the PolyBoard OPA PICs and the execution of the characterization process (shown not in scale): a) Raspberry Pi4 micro-computer serving as the central processing and orchestration component of the unit, b) Evaluation board of LTC2668-16 DAC from Linear Technology with 16 channels and 16-bit resolution, and c) Analog electronics boards designed by Optagon for the voltage-controlled provision of the currents that activate the heating electrodes (thermal phase shifters) of the PolyBoard PICs.

• Raspberry Pi4: Raspberry Pi4 (RPi4) [13] has been the micro-computing platform of choice for the development of the smart part of the control electronics unit. This has been due to the powerful processing capabilities it has and the multiple connectivity options it offers including general purpose inputs and outputs (GPIOs), Serial Peripheral Interface (SPI) ports, Inter-Integrated Circuit (I2C) ports, as well as more advanced connectivity options such as Universal Serial Bus (USB) ports and WiFi. The connectivity options that are used in our unit are the SPI ports for the communication of the controller with the DAC that controls in turn the analog current sources of the unit, and the USB port for the tentative connection of the controller with the IR camera that capture the profile of the emitted beam in real time. Apart from these connectivity options, the choice of the RPi4 as the central reference

point of the control electronics unit had to do with the availability of a highly functional version of Linux as operating system (Raspbian), the availability of ready-to-use drivers for the use of the SPI and the USB protocols, and the availability of ready-to-use editors and programming tools for the use of Python, which was qualified as the programming language of choice for the development of the firmware of the control electronics unit.

- LTC2668-16 DAC: The DAC of choice for the generation of the voltage signals that control the voltage-controlled operations of the unit has been the LTC2668-16 from Linear Technology [14]. It offers 16 channels with 16-bit resolution within the 0-10 V range with high operation robustness and reliability. Its evaluation board (see Figure 10b) offers on top of that an SPI interface for the connection of the DAC to a digital controller (the RPi4 here).
- Analog boards for current control and provision: The first generation of these analog boards (see Figure 10c) involved 8-channel circuits based on Bipolar Junction Transistors (BJTs) that could act as voltage-controlled voltage sources with high output current to the ohmic loads. They could thus support not only the operation of the heating electrodes in the PolyBoard platform with ohmic resistance in the range from 16 to 20 Ohm, but also the operation of the corresponding electrodes in the TriPleX platform (not relevant to the testing of the PolyBoard OPA PICs in the present report) with ohmic resistance up to 600 Ohm. Both in the more energy efficient case of the PolyBoard phase shifters and in the less efficient case of the TriPleX phase shifters, these analog circuits could easily provide currents up to 40 mA facilitating phase shifts in excess of 2π , and thus convenience in the configuration of the corresponding PICs and the identification of the optimum operation points. On the other hand, the fact that the circuits did act as voltage sources made necessary the knowledge of the resistance of the ohmic load that had to be operated. This knowledge could be easily obtained by a simple measurement at the two sides of each heating electrode off-chip.

The three constituent components that have been described above were combined inside a suitable package (see Figure 11) in order to serve as the electronics control unit for the operation of the PolyBoard OPA PICs and the execution of the relevant operation tests. The unit comprised one Raspberry Pi4 micro-computer, a single LTC2668-16 DAC evaluation board, and two analog PCBs. It could thus accommodate the control of 16 phase shifters, although the control of only 8 of them was necessary during the OPA experiments. It could also offer the possibility for connection to a display monitor via the HDMI port of the Raspberry Pi4 micro-computer, and connection to the IR camera, a keyboard and a mouse via the USB ports of the same micro-computer. The Graphical User Interface (GUI) that was developed for the operation of the OPA PICs is shown in Figure 12. This GUI was based on the Python programming language and offered: 1) The possibility to activate, de-activate and adjust the current (in mA) of each heating electrode (thermal phase shifter) of the PICs via a dedicated slider with well-defined limits for PIC protection, and 2) the possibility to



Figure 11: Picture of the control electronics unit for the operation of the PolyBoard OPA PICs at the final stages of its assembly consisting of a Raspberry Pi4 micro-computer, a DAC, analog boards for the provision and the control of the current to the heating electrodes (phase shifters) of the PICs, and a supply unit for the provision of the DC levels at the input of the various electronic components and boards. The only external electronic supply used for the powering of this unit is the 230V/50 Hz AC supply.

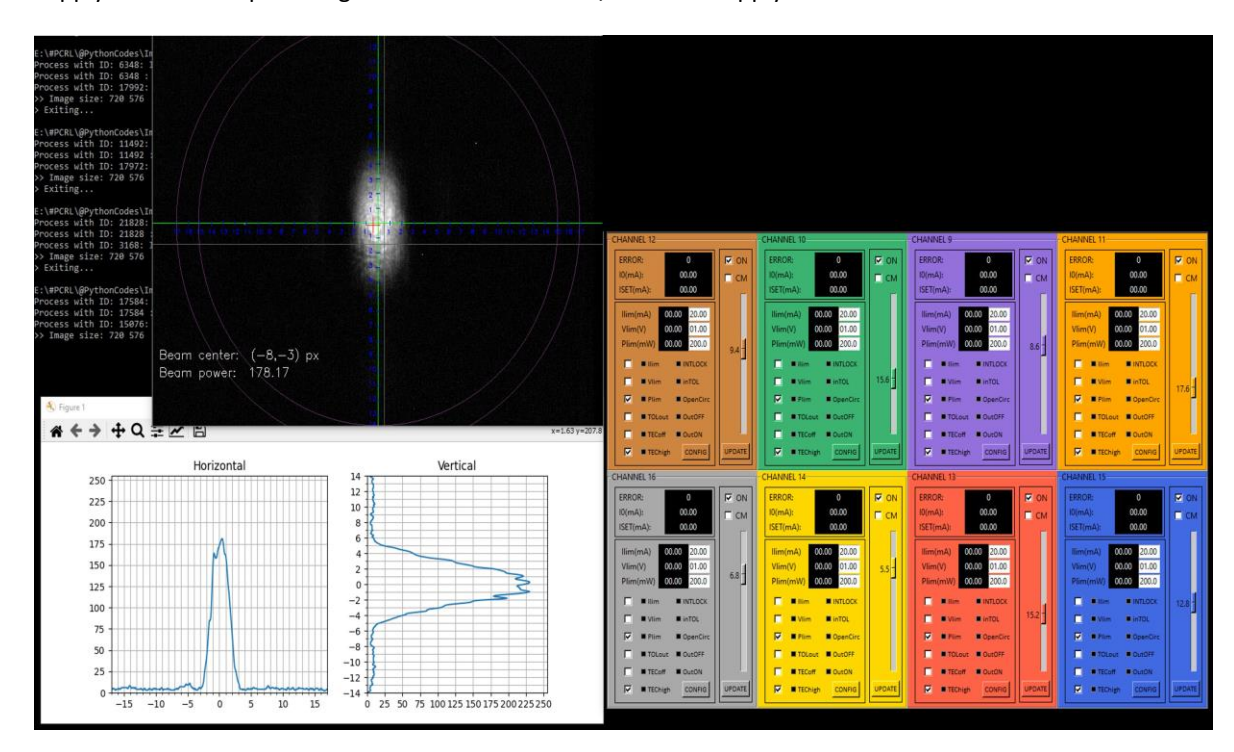


Figure 12: Graphical user interface for the control of the PolyBoard OPA PICs and for the execution of the characterization process that includes the acquisition and the processing of the beam profile.

D6.4: Development of control unit for the 2D optical phased array beam scanning system

acquire frames from the IR camera, and to process the corresponding values of each pixel via software-empowered application of specific processing functionalities such as averaging and fitting. It is noted that the design of the GUI using sliders was the design of choice for a quasi-static operation of the OPA during the characterization phase of the PolyBoard OPA PICs. Versions of the same software, where this part of the GUI was omitted in order to accelerate the communication between the electronics components and achieve an automated reconfiguration of the OPA as part of a beam scanning process were also developed and tested. Although the speed of the electronics could be much faster with these versions, it is noted that the scanning speed was rather low due to the fundamental limitation in the re-configuration speed of the thermal phase shifters on the PolyBoard platform (on the order of 1 kHz from a scanning point to the next one).



Figure 13: Picture of a PCB prepared by Optagon for the development of prototypes in its research and commercial activities based on design principles and components used in the control electronics unit of the OPA PICs in 3PEAT.

Finally, it is noted that the components that have been described above as the constituent components of the control electronics unit of the PolyBoard OPA PICs have been further developed by Optagon within the framework of other R&D activities, and constitute today a part of the technology basis of the company for the development of prototypes in its research and commercial operations. As a first example of this further development, Figure 13 presents a PCB that brings together a Raspberry Pi4 micro-computer and the required circuit for the use of two LTC2668-16 DACs. The 32 channels of the two DACs can be used for the provision of well-controlled voltage levels and the operation of voltage-controlled



Figure 14: Picture of a PCB assembly prepared by Optagon materializing a 16-channel high-performance voltage-controlled current source for the operation control of heating electrodes on various photonic integration platforms.

circuits. Two of them, which are in fact circuits that materialize current sources for the driving of laser diodes based on commercial Wavelength Electronics chips have been integrated and are part of the same PDB. The other 30 output channels remain available for connection to external components and circuits. As a second example, Figure 14 presents a vertical stack of 4 PCBs, each one of them materializing a quad array of voltage controlled current sources providing up to 50 mA to resistive loads up to 600 Ohm. By contrast to the voltage-controlled circuits that have been used in the control electronics unit of the OPA PICs, the circuits of Figure 14 operate as pure current sources, and provide to the ohmic loads the current that is defined by the input voltage independently from these loads.

2.2 Basic characterization results of the PolyBoard OPA PICs

The control electronics unit that has been presented in the previous paragraph was used for the basic characterization of the PolyBoard OPA PICs in the lab of ICCS. The present paragraph presents the setup for the characterization of the far-field radiation pattern of the PolyBoard PICs, and the main results that were obtained as the core outcome of this characterization. It is based to a large extent on the material that was published in the scientific publication (IEEE/OSA Journal of Lightwave Technology) achieved by Optagon, ICCS and FhG-HHI as part of the dissemination and exploitation plan of 3PEAT project [1].

Experimental setup: Figure 15 depicts the setup prepared by ICCS for the experimental investigation of the radiation pattern of the OPAs in the PolyBoard PICs. Within this setup,

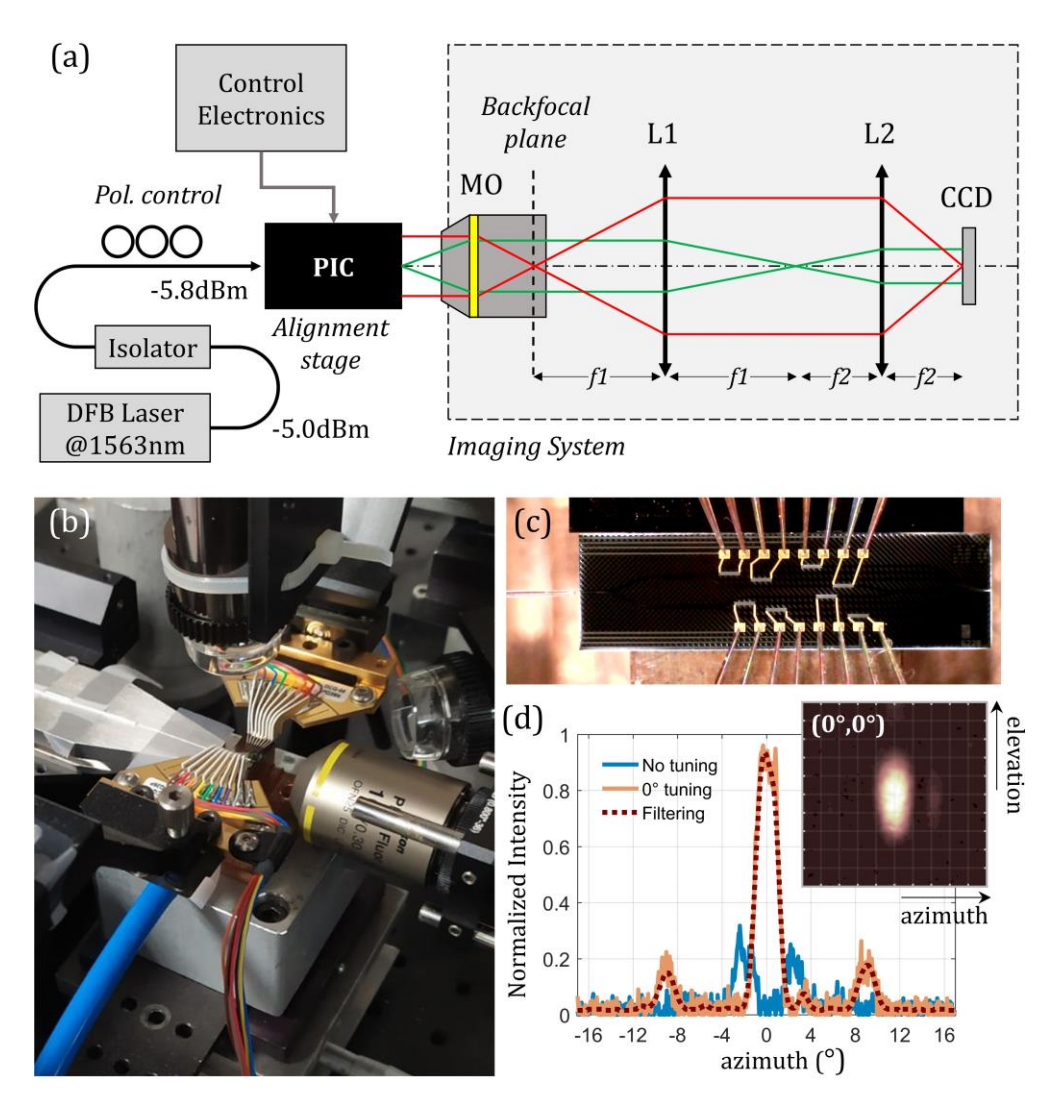


Figure 15: (a) Layout of experimental setup and Fourier imaging system for the characterization of the farfield of the PolyBoard OPA PICs. (b) Picture of the setup. (c) Close-up of a PolyBoard PIC with a 2×4 OPA. (d) Example image from a 2×4 OPA with 6 μ m lateral pitch. The beam is centred at 0° on both planes. The diagram depicts the plots related to the radiation intensity on the azimuthal plane when the phase shifters are off, when the phase shifters are tuned for emission at 0°, and when an additional filtering operation is applied.

a distributed feedback (DFB) laser provides a continuous wave (cw) at 1563 nm with -5.0 dBm output power. The light passes through an optical isolator and a polarization controller (PC), and is coupled to each PIC under test from the left-side of the PIC. It propagates further through the optical structures on-chip, is emitted from the edge-emitting waveguides on the right-hand side of the PIC, and is collected by a system of lenses that form a Fourier imaging system [15]. In such a system, the far-field is imaged at the back-focal (Fourier) plane of a microscope objective (MO), and is brought back to a sensor using a pair of lenses with an image ratio, which is defined by the focal lengths of the two lenses. The MO in the setup has a numerical aperture (NA) equal to 0.3. The two lenses L1 and L2 have focal lengths f1 and f2 equal to 100 and 50 mm, respectively. These lengths were carefully

selected so that the entire area of the sensor at the right end of the imaging system can be utilized for light detection. This sensor is in fact a 1/2" charge-coupled device (CCD) near NIR camera with 768 × 494 pixels and 8.4 μm × 9.8 μm pixel size. With this imaging system, emission angles from the OPAs up to 17° on the azimuthal plane and 14° on the elevation plane can be measured with resolution better than a tenth of degree. The emitted light that passes through the principal axis of the imaging system hits the center of the CCD sensor, and appears at the center of the captured image corresponding to a beam steering angle of 0° both on the azimuthal and the elevation plane. The light that is emitted towards the positive azimuthal angle corresponds to the right part of the image, while the light that is emitted towards the positive elevation angle corresponds to the upper part of the image. Prior to the installation of the imaging system in the setup, a careful characterization was carried out to create a pixel-to-angle mapping for the captured images. For this purpose, an auxiliary laser source with a collimated output beam was mounted on a rotational stage. The rotation axis of the stage was placed exactly at the position, where the OPAs at the endfacet of the PolyBoard PICs were expected to be in order to emulate the light emission conditions in the actual experiments. It is noted that the beam size of the auxiliary laser source was adequately small to yield a spot size of almost a single dot in our imaging system. Via the rotation of the collimated beam by a known angle, it was thus possible to calibrate the image acquisition process in terms of steering angle and light intensity, and to compensate for the small image distortion effects originating from our lens system. Finally, the light coupling into the PolyBoard PIC under test was accommodated by a 6-axis alignment station. The heating electrodes that adjust the phase of the individual AEs of the OPAs were controlled by the 8-channel current driver described in the previous paragraph. Two 16-pin probe heads with 50 µm pitch were additionally used to interface the controller with the chip pads.

Experimental results: The OPAs in all PolyBoard PICs were fabricated with random phase differences between the AEs, resulting in a random radiation pattern when the phase shifters are off (see Figure 15d). To overcome the randomness of this initial pattern, each PIC had to undergo a 2-step calibration process. In the first step, the required driving current for phase shift equal to 2π was precisely identified for each phase shifter (heating electrode). In the second step, appropriate phase shifts were applied on the individual waveguides in order to eliminate the phase differences between the AEs and maximize the radiation intensity at the direction of 0° on both the azimuthal and the elevation plane. After the execution of these steps, all information required for precise 2D beam scanning was known. In all PolyBoard PICs under test, the required current for 2π phase shift was found to be close to 20 mA for the bottom layer electrodes and close to 16 mA for their top layer counterparts. Figure 16 presents a comparison between experimental and simulation results as evidence for the potential of the 3D PolyBoard PICs to facilitate well-controlled

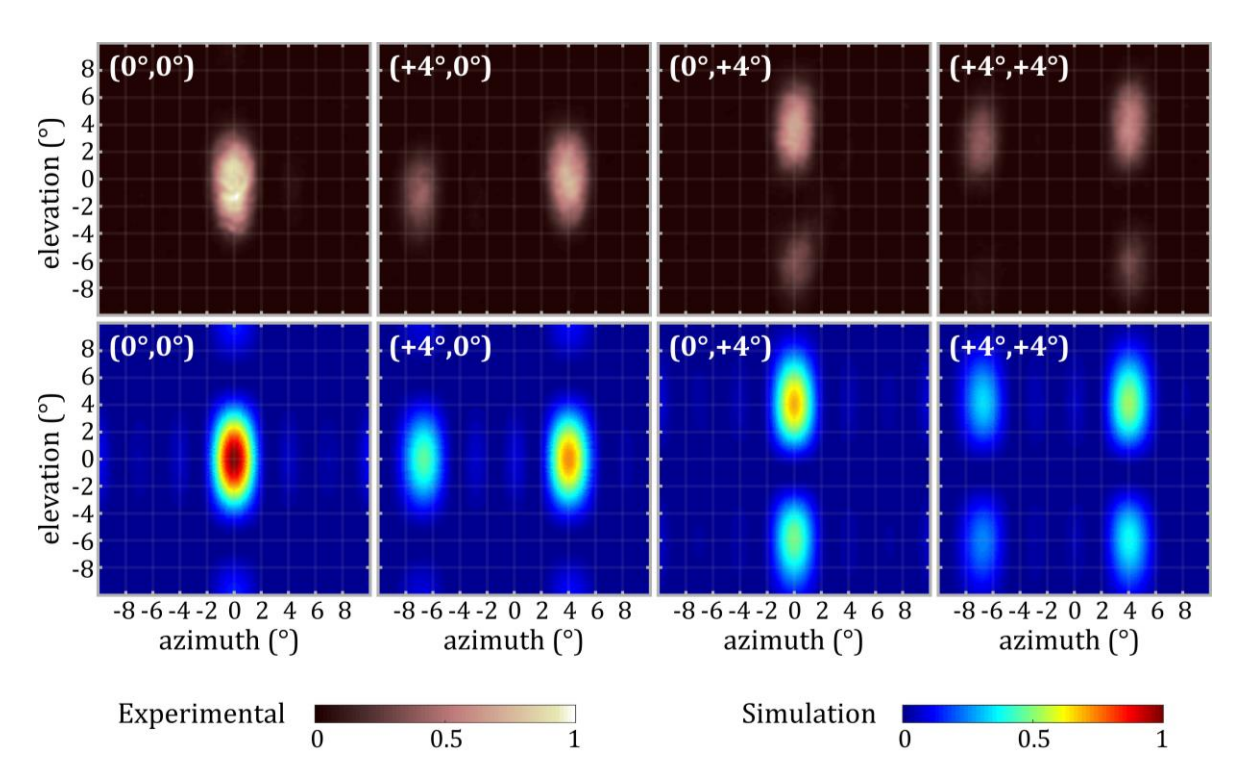


Figure 16: Comparison between the simulation (upper row) and the experimental (lower row) radiation patterns in the case of the 2×4 OPA with 8 μ m lateral pitch in four beam steering scenarios. The intended main lobe steering angle is displayed in each frame at the top-left. First column scenario: (0°, 0°). Second column scenario: (4°, 0°). Third column scenario: (0°, 4°). Fourth column scenario: (4°, 4°).

beam scanning on the azimuthal and the elevation plane. The experimental images (in the upper row) are from the testing of the 2×4 OPA with 8 µm lateral pitch, and the simulation results (in the lower row) are from the simulation of the far-field radiation of the same structure. Based on the curves in Figure 5a for 2 AEs with 7.2 μm pitch, and for 4 AEs with 8 µm pitch, the expected spacing between the main and the grating lobes in the radiation pattern of this OPA was approximately 9.9° in the vertical direction and 10.7° in the lateral direction. Four beam steering scenarios were investigated. The first one (shown in the first column) corresponds to intended beam direction at 0° both on the azimuthal and the elevation plane (0°, 0°). No grating lobes were present in the experimental image. The second scenario (shown in the second column) corresponds to intended beam direction at +4° on the azimuthal and 0° on the elevation plane (+4°, 0°). A grating lobe was present in this case at (-6.7°, 0°), as expected. The third scenario (shown in the third column) corresponds to intended beam direction at 0° on the azimuthal and +4° on the elevation plane (0°, +4°). The previous grating lobe was not present anymore, but a new one at (0°, -5.9°) was present, close to its expected position. Finally, the fourth scenario (shown in the last column) corresponds to intended beam direction at +4° both on the azimuthal and the elevation plane (+4°, +4°). In this case, grating lobes were present both in the lateral and vertical direction at azimuthal and elevation angles that were practically equal to the

expected ones. As evident from Figure 16, the experimental and the simulation images were remarkably similar. This similarity validated the 2D beam scanning concept of 3PEAT project, and demonstrated the quality of the fabricated 3D PolyBoard PICs.

Figure 17 presents an additional compendium of experimental images that validated further the beam scanning concept of 3PEAT and provided additional information about the presence of grating lobes in the radiation patterns of the PolyBoard OPA PICs. More specifically, Figure 17 presents two subgroups of images. The first one on the top is associated with the testing of a 2×4 OPA with 8 µm lateral pitch, while the second one in the bottom with the testing of a 2×4 OPA with 6 µm lateral pitch. Each subgroup includes 9 images that correspond to intended beam directions at -4°, 0° and +4° on the azimuthal and the elevation plane. Based on the curves of Figure 5a for 2 AEs with 7.2 µm pitch and for 4 AEs with 6 μm pitch, the expected spacing between the main and the grating lobes in the images of the second subgroup was approximately 9.9° in the vertical and 14.0° in the lateral direction. In both subgroups, the symmetry of the images with respect to the lateral and the vertical axis was evident in the case of symmetrical beam steering directions, which manifested the high performance quality and operation predictability of both OPAs. The spacing between the main and the grating lobes in the vertical direction was approximately 9.9° in all images of the first and the third row of both subgroups. This result was expected since the OPAs had the same number of AEs (2) and the same pitch (7.2 μm) in the vertical direction. In the lateral direction on the other hand, a significant difference was observed due to the different pitch between the two OPAs. While in the images of the first and the third column of the first subgroup (8 µm pitch) the spacing between the main and the grating lobes was 10.7°, in the corresponding images of the second subgroup (6 µm pitch) no grating lobes were present. The reason is that the grating lobes in this second subgroup were actually expected to have a spacing of 14° from the main lobe, and thus to appear at ±10° in the lateral direction, where they were strongly suppressed by the envelope of the single waveguide emitter.

Finally, Figure 18 presents data from a more in-depth analysis of experimental images. More specifically, Figure 18a presents the radiation intensity of the 2×4 OPA with 8 µm pitch, when the beam was scanned on the azimuthal plane from -6° to +6° with 2° angle step, and its elevation angle was kept 0°. The information associated with the images of the second row in the first subgroup of Figure 17 is thus included in Figure 18a. The distribution of the radiation intensity is shown for the slice of 0° elevation angle, as a function of the azimuthal angle. In a similar way, Figure 18b presents the radiation intensity of the same OPA, when the beam was scanned on the elevation plane from -4° to +4° with 2° angle step, and its azimuthal angle was kept 0°. The information associated with the images of the second column in the first subgroup of Figure 17 is included in Figure 18b. The distribution of the

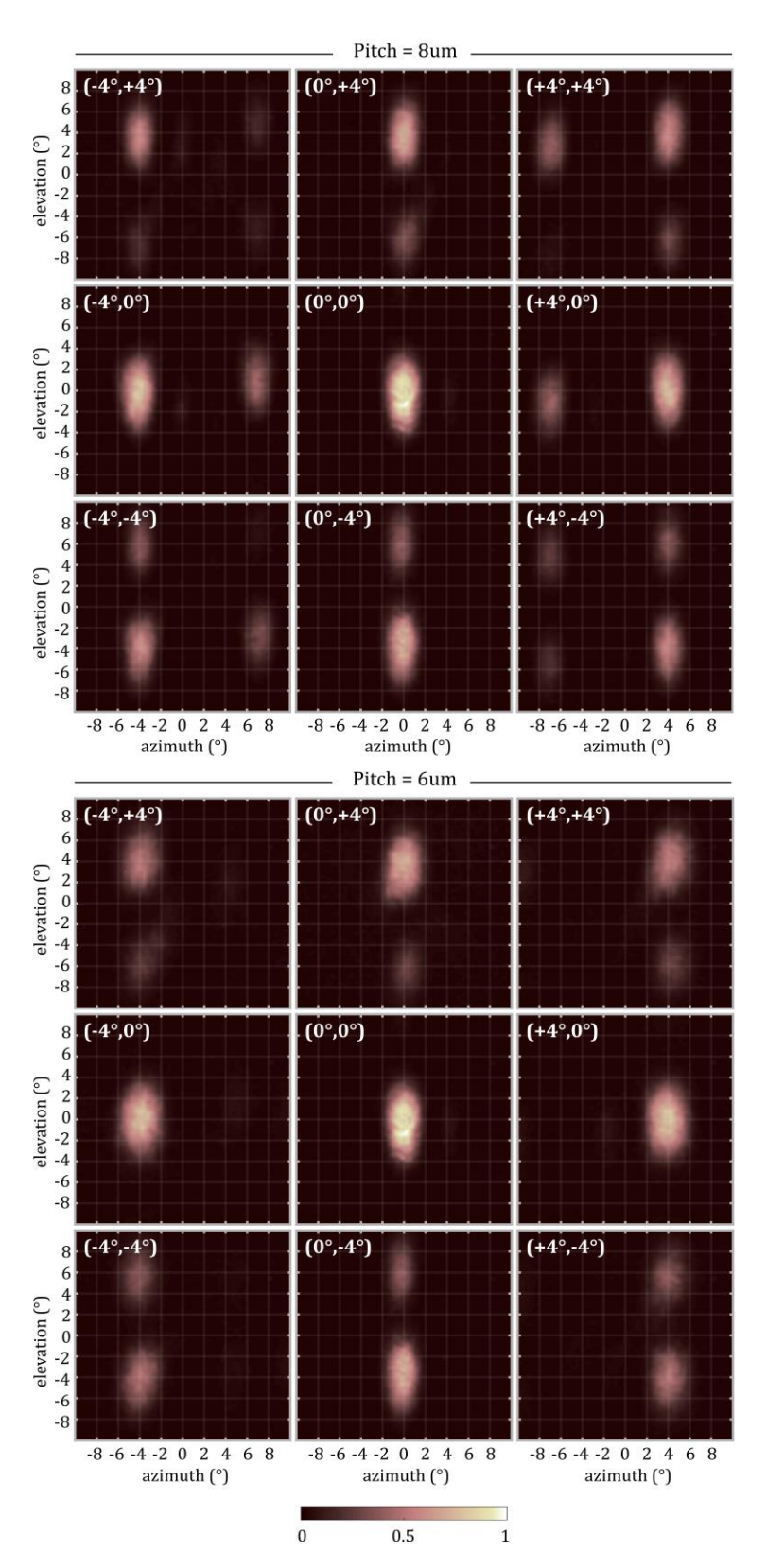


Figure 17: Experimentally captured images (radiation patterns) of the 2×4 OPAs with 8 μ m (upper subgroup) and 6 μ m (lower subgroup) lateral pitch. Within each subgroup, nine beam steering scenarios are presented corresponding to angles from -4° to +4° with 2° step on the azimuthal and the elevation plane.

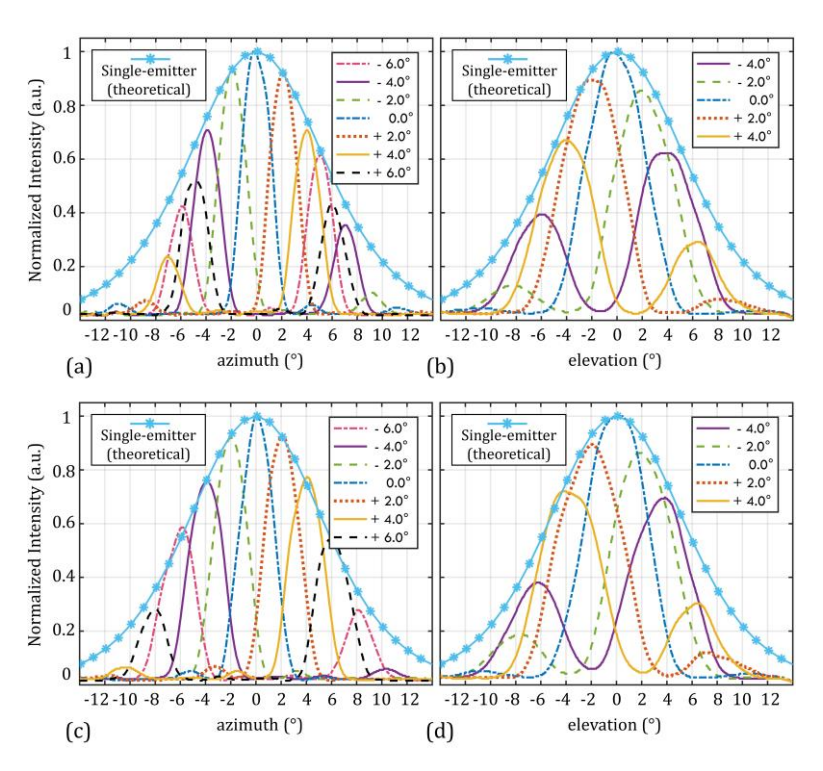


Figure 18: Analysis of experimental images from two 2×4 OPAs with 8 and 6 μ m lateral pitch. Eleven beam steering scenarios were investigated for each OPA corresponding to 0° elevation angle and azimuthal angle from -6° to +6° with 2° step, and to 0° azimuthal angle and elevation angle from -4° to +4° with 2° step: a) 8 μ m pitch: Intensity distribution on the azimuthal plane for 0° elevation angle. b) 8 μ m pitch: Intensity distribution on the elevation plane for 0° azimuthal angle. c) 6 μ m pitch: Intensity distribution on the azimuthal plane for 0° elevation angle. d) 6 μ m pitch: Intensity distribution on the elevation plane for 0° azimuthal angle. In all diagrams, the theoretical intensity distribution of the PolyBoard edge-emitting waveguide is drawn as envelope.

radiation intensity is shown for the slice of 0° azimuthal angle, as a function of the elevation angle. Finally, Figure 18c and Figure 18d present the same information as Figure 18a and Figure 18b, but for the radiation intensity of the 2×4 OPA with 6 μ m pitch. In all these figures, the theoretical radiation intensity of the single edge-emitting waveguide has been drawn to make obvious that its distribution serves as an envelope that suppresses the OPA lobes at large angles. As observed, the matching between the theoretical envelopes and the experimental data was very good in all cases, proving again the consistency of the results. The angular spacings between the main lobes and their companion grating lobes were also in good agreement with the theoretical values, as these could be extracted from Figure 5a, as already described. Finally, more careful inspection of the relevant intensity levels between the main lobes and their companion grating lobes in Figure 18a to Figure 18d reveals that the experimental data were also aligned with the expected values from Figure 5b to Figure 5d. As example, in the case of an OPA with 4 AEs and 6 μ m pitch, the theoretical 3dB clearance from Figure 5b is 10.8°. The curves in Figure 18c for beam direction at $\pm 4^{\circ}$ and $\pm 6^{\circ}$ revealed that the experimental 3 dB clearance on the azimuthal plane was much

larger than 8°, but still smaller than 12°. Use of simple fitting calculations indicate that the actual 3 dB clearance was in fact very close to the theoretical one. The same conclusion about the agreement of the experimental and the theoretical data with respect to the angular clearance could be drawn by a similar inspection of the other curves in Figure 18.

3. Development of control electronics for the final OPA PICs of 3PEAT project

The present section presents the preparations of Optagon for the development of the control electronics unit that will be able to control the operation of the OPA in the final module of 3PEAT (Module-6), whenever this module will be ready for testing after the official end of the project. In the first paragraph of the section, we present the structure of the OPA in Module-6, and we outline the basic differences from the OPA structure in the PolyBoard OPAs that have already tested. In the second paragraph, we describe the necessary changes in the driving components of the control electronics unit and the PCBs that were developed by Optagon to this end. Finally, the third paragraph describes the changes in the software that are currently taking place in order to make easier the calibration process of the larger and more complex OPA of the final 3PEAT module.

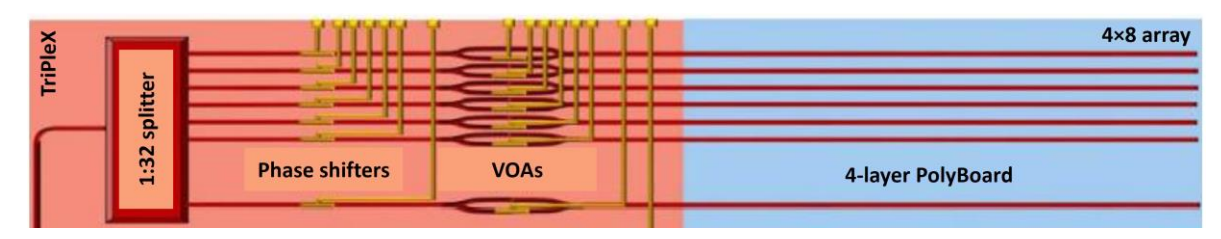


Figure 19: Circuit schematic of the OPA that will be part of the final 3PEAT module (Module-6). The 4×8 OPA with edge-emitting waveguides will span across two photonic integrated platforms (TriPleX and PolyBoard). The two platforms will be hybridly integrated to form a single hybrid PIC. The PolyBoard part will have 4 waveguiding layers with 32 edge-emitting waveguides acting as AEs, and a set of vertical MMI couplers for light transition from the seed to each one of the waveguiding layers. The TriPleX part will comprise a set of static couplers operating together as a 1:32 splitter, a set of 32 phase shifters based on PZTs and a set of 32 VOAs, realized as MZIs with 2 phase shifters each. The phase shifters of the MZIs will be based again on PZTs.

3.1 Design of final OPA PICs of 3PEAT project

During the course of the project and considering the challenges in the development of the multi-layer PolyBoard PICs, it was decided that the corresponding module of 3PEAT project (Module-6) will be equipped with a 4×8 OPA. Although this OPA is smaller than the 16×16 OPA that was originally planned, it still offers high resolution on the azimuthal plane and keeps high the complexity of the design. Compared to the OPAs in the PolyBoard PICs, the OPA of Module-6 has the main difference that it spans across two platforms, which are combined to form a single hybrid PIC. The first one is the TriPleX platform, which as far as the OPA is concerned comprises a set of optical splitters for the distribution of the input light among the 32 AEs of the OPA, a set of 32 phase shifters for controlling the relative

phase between the AEs, and a set of 32 Mach-Zehnder Interferometers (MZIs) acting as variable optical attenuators (VOAs) for ensuring the homogeneity in terms of optical power in the excitation of the AEs. Each MZI will have two phase shifters residing at either its branch, and operating in a push-pull mode to apply the necessary attenuation to the input signal. It is noted that both the phase shifters for the control of the relative phase between the AEs, and the phase shifters of the VOAs will be based on PZT elements on the TriPleX platform. These PZT elements represent capacitive loads and have very different driving requirements from the heating electrodes on the TriPleX or on the PolyBoard platform. They thus require a different design and a different set of driving PCBs in their control electronics unit compared to the PolyBoard OPA PICs presented in the previous sections.

3.2 Development of control electronics

Different versions of electronic units for the driving of PZT elements have been developed by Optagon in 3PEAT with the aim to cover different combinations of specs and needs regarding the reconfiguration speed, the capacitance, the Vpi and the number of the PZTs in the various PICs of the project. These four parameters (speed, capacitance, Vpi and number of elements) create a very large space that cannot be satisfactorily addressed by a single driver design. As a matter of fact, the top-top design of PZTs on the TriPleX platform represents a PZT design with low capacitance (100 pF) that can support high modulation with acceptable power consumption. However, this low capacitance comes at the expense of ultra-high Vpi (120-200V), which is the required voltage for phase shift equal to pi. At the other end, the top-bottom design of PZTs represents a design with high piezoelectric efficiency, which results in low Vpi values (15-30 V). However, the capacitance in this case is ultra-large (4-5 nF) making impossible the support of high reconfiguration speeds. Moreover, yield issues are more often present making this specific design less suitable for large-scale PICs with large number of PZT-based phase shifters.

Given this variation in the operation parameters of the PZTs, Optagon has developed three main driving units. The first one is illustrated in Figure 20. It has been designed to provide high-bandwidth (>10 MHz), and support the operation of the low-capacitance PZTs in applications, where high-speed modulation of the PZTs is required. By virtue of its careful design this unit is capable of an output peak-to-peak voltage in excess of 70 Vpp, which represents a clear achievement for this kind of capacitive loads and bandwidth regimes. Figure 21 presents two representative screenshots from the testing of this driver unit. The screenshot on the left presents the output signal with 71.2 Vpp amplitude when the unit is fed with a 2.5 MHz sinusoidal signal. The screen on the right presents on the other hand the output signal with 70.4 Vpp amplitude when the unit is fed with a sawtooth signal at 2.5 MHz repetition rate. Given that the sawtooth function is extremely demanding in terms of bandwidth, the high quality of the output waveform confirms the high performance of the

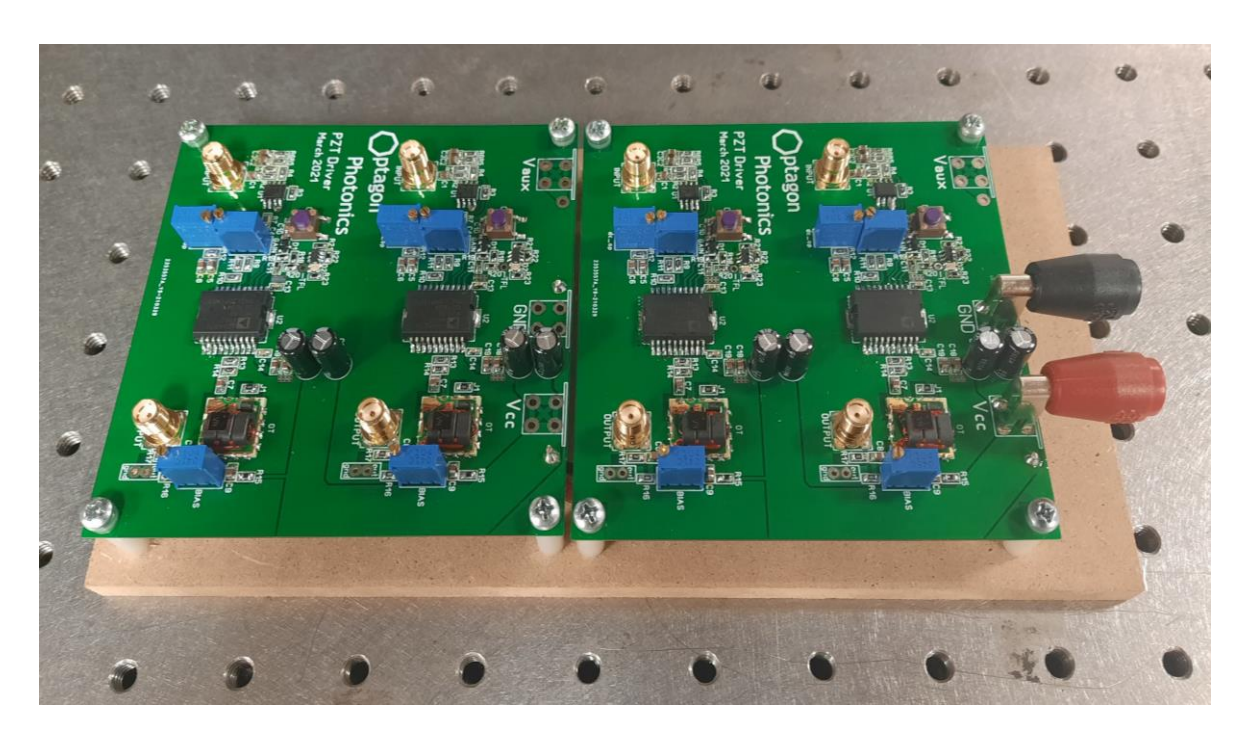


Figure 20: Picture of the twin PCBs that implement a quad-channel driver for PZTs with low capacitance (up to approximately 300 pF) with high output amplitude (>70 Vpp) and high bandwidth (>10 MHz).





Figure 21: Screenshots from the testing of the driver unit of Figure 20. (Left): Output signal with 71.2 Vpp in the case of sinusoidal input at 2.5 MHz. (Right): Output signal with 70.4 Vpp in the case of a sawtooth input signal at 2.5 MHz.

driving unit. It is noted that in both cases, the input signals were provided by a high-speed DAC from Texas Instruments connected to a Field Programmable Gate Array (FPGA). No pre-amplification stage was required in between thanks to the high gain of the driving unit. It is also noted that the specific driving unit was successfully used as a 4-channel driver for the operation of the 4-branch serrodyne shifter of the laser Doppler vibrometer of 3PEAT (Module-4). The experimental setup and the results that were obtained during the characterization of Module-4 have been reported in 3PEAT deliverable D6.2. The electrical signals at the input of the 4-channel driver were 2.5 MHz sinusoidal signals with 90° differential phase shift. The peak-to-peak amplitude of each signal at the output was close to 70 V. Although this value was much lower than the Vpi of the PZTs, it was already enough

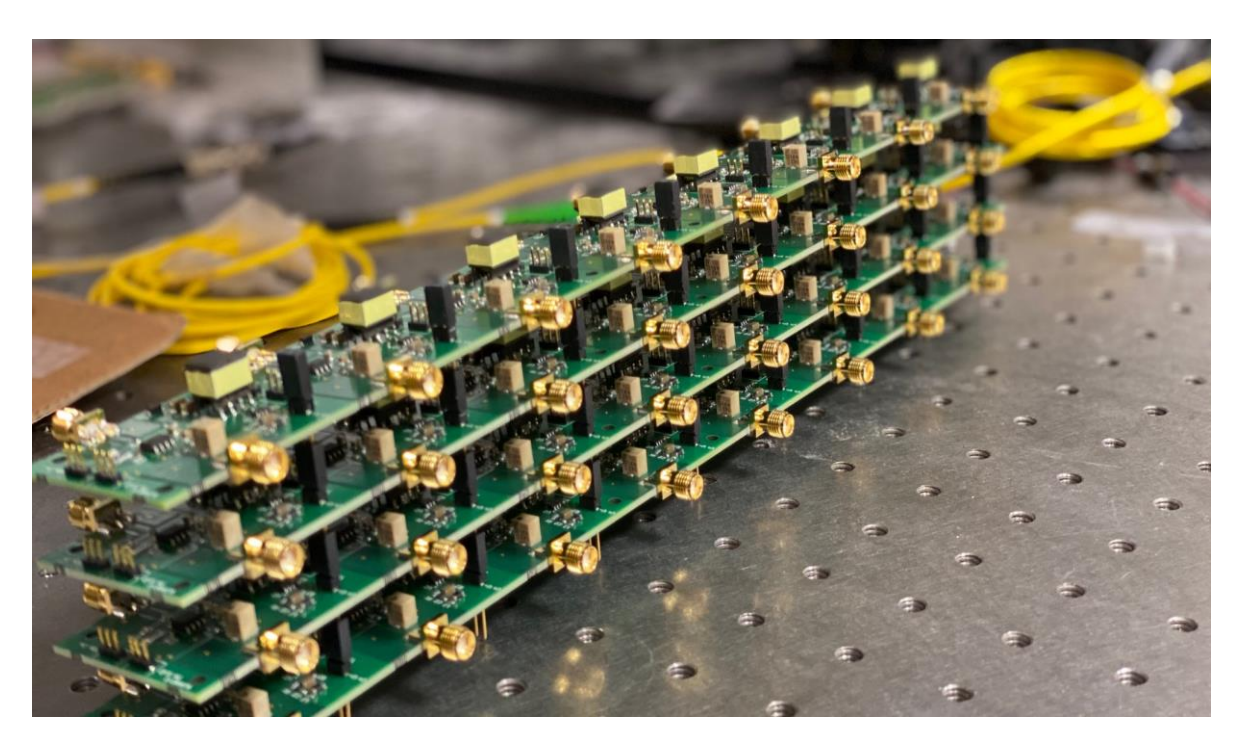


Figure 22: Picture of the unit that implements a 32-channel driver for PZTs with high capacitance (> 1 nF) with high output amplitude (60 Vpp) and moderate bandwidth (100 kHz).

to accommodate high operation quality thanks to the operation principles of the 4-branch serrodyne shifter [16].

Figure 22 presents on the other hand the picture of an alternative driving unit that has been developed by Optagon, and can support the modulation of PZTs with significantly higher capacitance (>1 nF), but at significantly lower modulation speeds (100 kHz). The output peak-to-peak amplitude in these case is approximately 60 Vpp. For PZTs with capacitance closer to 5 nF rather than to 1 nF, the same amplitude level can be achieved at lower modulation speeds (30-40 kHz).

Finally, Figure 23 presents the control electronics unit that has been qualified for the baseline operation and testing of the OPA unit of Module-6. It implements a 160-channel PZT driver capable of supporting a quasi-static operation of the PZTs and providing ultrahigh output amplitude up to 300 Vpp for any capacitance value. The unit is based on the combination of five HV257 integrated circuits (ICs) from Microchip, each implementing a 32-channel sample-and-hold amplifier with a linear Vout/Vin gain of 70. Each IC is equipped with a 5-to-32 decoder, which is accessible to the central micro-computer platform of the unit (RPi4), and controls the process for the refreshment of the input of each amplification channel. In more detail, the decoder receives as input a set of 5 digital inputs (E0, E1, E2, E3 and E4), which define which one of the 32 channels will be refreshed. An additional digital input (EN) acts as the enabling signal, opening a time-slot for the use of the input signal (Vsig) as the input for the setting of the output amplitude level of the specific signal. This

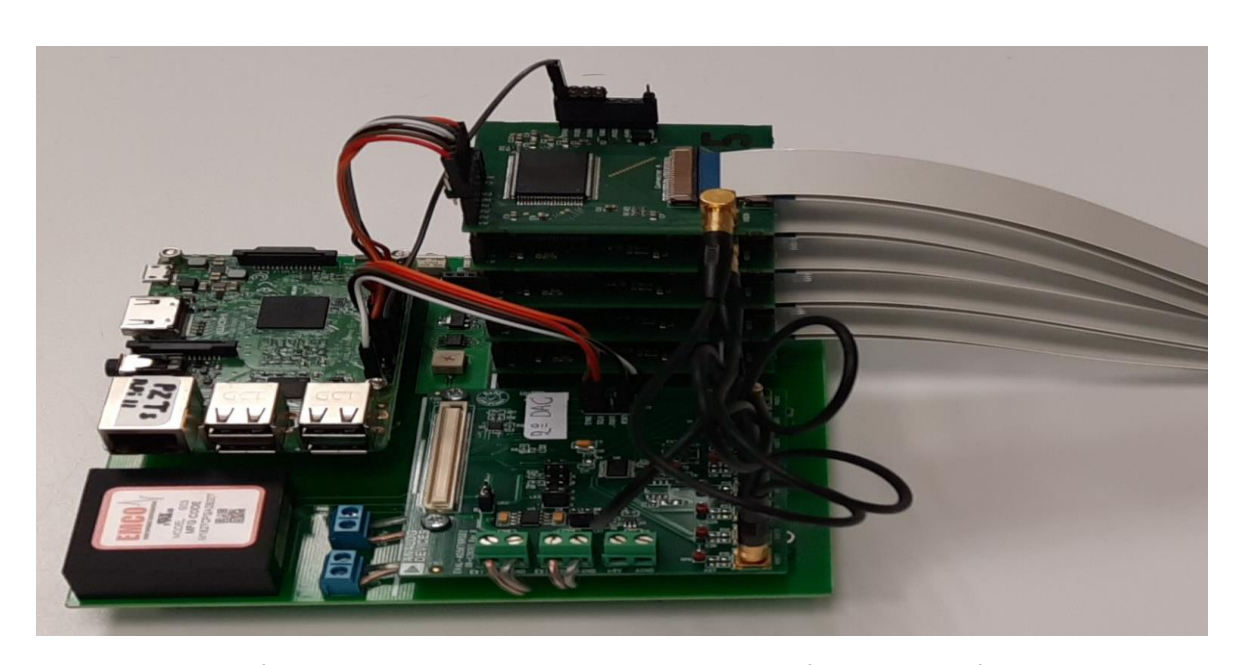


Figure 23: Picture of the unit that implements a 160-channel driver for operation of PZTs with ultra-high output amplitude (up to 300 Vpp) at quasi-static operation (<1 kHz). The unit shown here contains the digital part (RPi micro-computer, the DAC, and the final driving PCBs each based on the HV257 IC from Microchip, which implements a 32-channel high-voltage sample-and-hold amplifier array.

process is cyclic, enabling the continuous refreshment of all amplification channels. It is noted that the Vsig is provided by a DAC, which is also part of the control electronics unit, and can be reconfigured at high speed in order to accommodate this refreshment process. By virtue of this control electronics unit, it will be made possible to control the 96 PZTs in the TriPleX part of the OPA PIC of Module-6 for the control of the relative phase and amplitude of the AEs of the 4×8 OPA.

3.3 Development of calibration process and algorithms

The transition from the testing of the small-scale 2×4 OPA PICs to the testing of the large-scale 4×8 OPA PICs is expected to present additional difficulties in the initialization of the OPA, which is equivalent to the formation of an optical beam (with dimensions defined by the number of the AEs) at 0° azimuthal and 0° elevation angle. Provided that this initialization can be achieved, the configuration of the OPA for beam steering to any angle on the azimuthal and the elevation plane can be easy and trivial. The initialization step during the testing of the 2×4 OPAs could be achieved in an intuitive way by adjusting the driving currents through the thermal phase shifters of the PICs and observing the light distribution on the two scanning planes (azimuth and elevation) with the help of the CCD camera. As already mentioned however, this intuitive process is expected to be time-consuming and problematic in the case of the much larger 4×8 OPAs.

In order to address the challenge of the initialization process Optagon is investigating in collaboration with ICCS a number of gradient descent algorithms for the accommodation of

the initialization process in OPAs, implementing different optimization strategies for the configuration of the phase shifters. In all cases, the main objective of the optimization algorithm is to reach the target initialization state with minimum risk to get trapped in local maxima and with satisfactory time-efficiency in order to avoid long initialization loops. First results at the simulation level (MATLAB and Python) are promising, while next steps involve the experimental validation of these algorithms with the help of a direct feedback loop from the CCD camera to the micro-computer platform (RPi4) of the control electronics unit.

Conclusions

The present document has reported on the development of the control electronics that have accommodated the operation and the testing of the OPA PolyBoard PICs of 3PEAT project. The development of these electronics followed the modelling of the 2D OPAs with edge-emitting waveguides, the design of the PolyBoard PICs with two waveguiding layers and 2×4 OPAs, and the development of the relevant testbed with a CCD camera for realtime acquisition of the emitted beam profile. The control electronics unit has been equipped with a central micro-computer platform for the orchestration of the OPA operation (i.e. control of the drivers, and acquisition and processing of the beam position and profile) and the provision of a handy user interface for the execution of the testing process. The drivers in this unit were designed to drive the thermal phase shifters on the PolyBoard PICs for the adjustment of the relative phase between the AEs of the OPAs. On the other hand the control unit that has been developed for the operation and the testing of the 4×8 OPA in the final module of 3PEAT (Module-6) comprises drivers for the PZTs in the TriPleX part of Module-6 that will act as phase shifters for the adjustment of the relative phase and amplitude between the AEs of the OPA. Finally work on the development of calibration algorithms based on the gradient descent optimization algorithm is done in order to enable the calibration of the 4×8 OPA without a time-consuming manual process.

Statement on exploitation potential and activities

The present document summarizes a large part of the technology developments led by Optagon within 3PEAT project. These developments had substantial impact on the consolidation of the business plan of Optagon as a young SME, on the development of its baseline technology with the aim to develop and commercialize meaningful products, and on the conduction of efforts for the development of intellectual property (IP). In detail:

 In alignment with its work in 3PEAT, Optagon identified and highlighted the development of control electronics for the operation of large-scale PICs as one of its main business areas.

- Within 3PEAT, Optagon developed technology and prototypes that constituted the basis for the design of driving electronics products for operation of large-scale PICs and support of experimentation in labs. Commercialization of these products is expected after the conclusion of 3PEAT project.
- Within 3PEAT, Optagon developed the baseline technology that makes possible the development and combination of smart software with its driving electronics.
- Finally, in alignment with its work on the modelling, design, and operation control of OPAs, Optagon filed an international Patent Cooperation Treaty (PCT) application on 29/01/2022 with application number PCT/IB2022/050789.

References

- Raptakis, L. Gounaridis, M. Weigel, M. Kleinert, M. Georgiopoulos, E. Mylonas, P. Groumas, C. Tsokos, N. Keil, H. Avramopoulos, and Ch. Kouloumentas, "2D Optical Phased Arrays for Laser Beam Steering Based On 3D Polymer Photonic Integrated Circuits," in Journal of Lightwave Technology, vol. 39, no. 20, pp. 6509-6523, Oct 2021.
- 2. X. Sun, L. Zhang, Q. Zhang, and W. Zhang, "Si Photonics for Practical LiDAR Solutions," Applied Sciences, vol. 9, no. 20, p. 4225, Oct. 2019.
- Christopher V. Poulton, Ami Yaacobi, David B. Cole, Matthew J. Byrd, Manan Raval, Diedrik Vermeulen, and Michael R. Watts, "Coherent solid-state LIDAR with silicon photonic optical phased arrays," Opt. Lett. 42, 4091-4094 (2017).
- 4. C. V. Poulton et al., "Long-Range LiDAR and Free-Space Data Communication With High-Performance Optical Phased Arrays," in IEEE Journal of Selected Topics in Quantum Electronics, vol. 25, no. 5, pp. 1-8, Sept.-Oct. 2019, Art no. 7700108, doi: 10.1109/JSTQE.2019.2908555.
- 5. S. Chung, H. Abediasl and H. Hashemi, "A Monolithically Integrated Large-Scale Optical Phased Array in Silicon-on-Insulator CMOS," in IEEE Journal of Solid-State Circuits, vol. 53, no. 1, pp. 275-296, Jan. 2018, doi: 10.1109/JSSC.2017.2757009.
- 6. Fu, X. J., Yang, F., Liu, C. X., Wu, X. J., Cui, T. J., "Terahertz Beam Steering Technologies: From Phased Arrays to Field-Programmable Metasurfaces" Adv. Optical Mater. 2020, 8, 1900628. https://doi.org/10.1002/adom.201900628
- M.J.R. Heck, "Highly integrated optical phased arrays: photonic integrated circuits for optical beam shaping and beam steering," Nanophotonics, vol. 6, no. 1, 2017, pp. 93-107. https://doi.org/10.1515/nanoph-2015-0152.
- 8. A. Hosseini, D. Kwong, Y. Zhang, S.A. Chandorkar, F. Crnogorac, A. Carlson, B. Fallah, S. Bank, E. Tutuc, J. Rogers, R.F.W. Pease, R.T. Chen, "On the fabrication of three-dimensional silicon-on-insulator based optical phased array for agile and large angle laser beam steering systems," Journal of Vacuum Science & Technology B, Nanotechnology and Microelectronics: Materials, Processing, Measurement, and Phenomena, 28(6), C6O1-C6O7 (2010).

- 9. S. Yoo, B. Guan, and R. Scott, "Heterogeneous 2D/3D photonic integrated microsystems," Microsyst Nanoeng 2, 16030 (2016). https://doi.org/10.1038/micronano.2016.30
- Z. Zhang, D. Felipe, V. Katopodis, P. Groumas, Ch. Kouloumentas, H. Avramopoulos, J.-V. Dupuy, A. Konczykowska, A. Dede, A. Beretta, A. Vannucci, G. Cangini, R. Dinu, D. Schmidt, M. Moehrle, P. Runge, J.-H. Choi, H.-G. Bach, N. Grote, N. Keil, M. Schell, "Hybrid Photonic Integration on a Polymer Platform," Photonics 2015, 2, 1005-1026. https://doi.org/10.3390/photonics2031005.
- 11. M. Nuck et al., "Low-Loss Vertical MMI Coupler for 3D Photonic Integration," 2018 European Conference on Optical Communication (ECOC), Rome, Italy, 2018, pp. 1-3, doi: 10.1109/ECOC.2018.8535479.
- 12. Antenna Theory: Analysis and Design (3rd Edition) (John Wiley & Sons, 2005) Author: Constantine A. Balanis.
- 13. https://www.raspberrypi.com/products/raspberry-pi-4-model-b/
- 14. https://www.analog.com/en/products/ltc2668.html#product-overview
- 15. Nicolas Le Thomas, Romuald Houdré, Maria V. Kotlyar, David O'Brien, and Thomas F. Krauss, "Exploring light propagating in photonic crystals with Fourier optics," J. Opt. Soc. Am. B 24, 2964-2971 (2007).
- 16. 3PEAT deliverable report D6.2: Development of basic control unit for the LDVs and evaluation of the first LDV with integrated PZT modulator (Module-4) using bench-top and system tests.

List of Figures

Figure 1: Fundamental 3PEAT concept for the development of 2D OPAs based on PolyBoard PICs with multiple waveguiding layers and vertical MMI couplers for light coupling between the adjacent waveguiding layers. Edge emitting single-mode waveguides serve as AEs at the end-facet of each PIC. The cladding material is omitted in the representation for clarity. A 4×4 OPA is shown as example. Any layer can be used as seed layer. Vertical couplers that couple directly the input light to the target layer without involving the intermediate ones can be alternatively used. Inset: Close view of a vertical MMI coupler followed by a lateral one
Figure 2: a) Coordinate system and geometry for the modelling of the edge-emitting PolyBoard waveguide as an aperture antenna using the Field Equivalence Principle (FEP), and b) Normalized radiation intensity of the edge-emitting PolyBoard waveguide on the azimuthal and the elevation plane
Figure 3: a) Coordinate system and geometry for the modelling of OPAs with edge-emitting waveguides in PolyBoard PICs, and b) Angular spacing between the main and the grating lobes of the AF (squared) in a linear OPA as a function of the pitch. Results are not PolyBoard specific. Inset: Example AF (squared) corresponding to a linear OPA with 4 AEs, 8 μm pitch and 0° steering angle
Figure 4: a) Exemplary radiation intensity of two linear PolyBoard OPAs on the azimuthal plane: The first one (Case 1) has 4 AEs, 8 μ m pitch and direction at +4°, and the second one (Case 2) has 8 AEs, 6 μ m pitch and direction at -4°. b) FWHM of the main lobe of the radiation intensity as a function of the pitch for different number of AEs and steering angles13
Figure 5: Radiation intensity of linear PolyBoard OPAs on the azimuthal plane: Angular clearance, wherein the main lobe of the radiation pattern is higher than any grating lobe by: a) 0 dB, b) 3 dB, c) 6 dB, and d) 10 dB13
Figure 6: Simulation study for the estimation of the crosstalk between two PolyBoard waveguides: a) Pattern for 100 μ m propagation, b) TE excitation of the two waveguides, and c) Output fields with dominant Ex component at z = 100 μ m. The three diagrams correspond to 7 μ m waveguide pitch, -30° phase in the excitation of waveguide 1, and 0° phase in the excitation of waveguide 2
Figure 7: a) Amplitude perturbation in the output field of waveguide 2 ($z = 100 \mu m$) due to the phase variation in the excitation of waveguide 1 (see Figure 6a). The 12 curves correspond to excitation phase from -180° to +150° with 30° step. b) Main results: Amplitude and phase perturbation at waveguide 2 output as a function of the pitch. The values are for the center of waveguide 2 ($x = 0$, $y = 0$).

Figure 8: Far-field radiation intensity of two edge-emitting PolyBoard waveguides with relative phases that lead to beam steering at 4° on the azimuthal plane. The diagrams correspond to waveguide spacing equal to: a) 4μ m, b) 5μ m, c) 6μ m, and d) 8μ m. The two curves in each diagram correspond to different simulation methods. The method of the blue solid curve does not take into account the optical crosstalk between the two waveguides, whereas the method of the red-dashed curve does. The difference between the two curves reveals the impact of the crosstalk on the radiation pattern for the respective waveguides spacing.
Figure 9: a) Mask layout for the fabrication of 2×4 OPAs with 10 µm lateral and 7.2 vertical pitch in 2-layer PolyBoards, and b) Photograph of a respective PolyBoard PIC (top-view). The tags (L or U) next to each heating electrode indicate, whether the particular electrode is used for the control of a waveguide at the lower or the upper layer of the 2-layer PolyBoard PIC c) Micro-photograph of the end-facet of the same PIC, where the edge-emitting waveguides that act as the optical AEs of the OPA are clearly visible
Figure 10: Main constituent components of the control electronics unit that was developed for the operation of the PolyBoard OPA PICs and the execution of the characterization process (shown not in scale): a) Raspberry Pi4 micro-computer serving as the central processing and orchestration component of the unit, b) Evaluation board of LTC2668-16 DAC from Linear Technology with 16 channels and 16-bit resolution, and c) Analog electronics boards designed by Optagon for the voltage-controlled provision of the currents that activate the heating electrodes (thermal phase shifters) of the PolyBoard PICs
Figure 11: Picture of the control electronics unit for the operation of the PolyBoard OPA PICS at the final stages of its assembly consisting of a Raspberry Pi4 micro-computer, a DAC, analog boards for the provision and the control of the current to the heating electrodes (phase shifters) of the PICs, and a supply unit for the provision of the DC levels at the input of the various electronic components and boards. The only external electronic supply used for the powering of this unit is the 230V/50 Hz AC supply
Figure 12: Graphical user interface for the control of the PolyBoard OPA PICs and for the execution of the characterization process that includes the acquisition and the processing of the beam profile
Figure 13: Picture of a PCB prepared by Optagon for the development of prototypes in its research and commercial activities based on design principles and components used in the control electronics unit of the OPA PICs in 3PEAT23
Figure 14: Picture of a PCB assembly prepared by Optagon materializing a 16-channel high- performance voltage-controlled current source for the operation control of heating electrodes on various photonic integration platforms

rigure 15: (a) Layout of experimental setup and Fourier imaging system for the characterization of the far-field of the PolyBoard OPA PICs. (b) Picture of the setup. (c) Close-up of a PolyBoard PIC with a 2×4 OPA. (d) Example image from a 2×4 OPA with 6 µm lateral pitch. The beam is centred at 0° on both planes. The diagram depicts the plots related to the radiation intensity on the azimuthal plane when the phase shifters are off, when the phase shifters are tuned for emission at 0°, and when an additional filtering operation is applied.
Figure 16: Comparison between the simulation (upper row) and the experimental (lower row) radiation patterns in the case of the 2×4 OPA with 8 μ m lateral pitch in four beam steering scenarios. The intended main lobe steering angle is displayed in each frame at the top-left. First column scenario: (0°, 0°). Second column scenario: (4°, 0°). Third column scenario: (0°, 4°). Fourth column scenario: (4°, 4°)
Figure 17: Experimentally captured images (radiation patterns) of the 2×4 OPAs with 8 μm
(upper subgroup) and 6 μ m (lower subgroup) lateral pitch. Within each subgroup, nine beam steering scenarios are presented corresponding to angles from -4° to +4° with 2° step on the azimuthal and the elevation plane29
Figure 18: Analysis of experimental images from two 2×4 OPAs with 8 and 6 μm lateral pitch.
Eleven beam steering scenarios were investigated for each OPA corresponding to 0°
elevation angle and azimuthal angle from -6° to +6° with 2° step, and to 0° azimuthal angle
and elevation angle from -4° to +4° with 2° step: a) 8 μm pitch: Intensity distribution on the
azimuthal plane for 0° elevation angle. b) 8 μm pitch: Intensity distribution on the elevation
plane for 0° azimuthal angle. c) 6 μm pitch: Intensity distribution on the azimuthal plane for
0° elevation angle. d) 6 μm pitch: Intensity distribution on the elevation plane for 0°
azimuthal angle. In all diagrams, the theoretical intensity distribution of the PolyBoard edge-
emitting waveguide is drawn as envelope30
Figure 19: Circuit schematic of the OPA that will be part of the final 3PEAT module (Module-
6). The 4×8 OPA with edge-emitting waveguides will span across two photonic integrated
platforms (TriPleX and PolyBoard). The two platforms will be hybridly integrated to form a
single hybrid PIC. The PolyBoard part will have 4 waveguiding layers with 32 edge-emitting
waveguides acting as AEs, and a set of vertical MMI couplers for light transition from the
seed to each one of the waveguiding layers. The TriPleX part will comprise a set of static
couplers operating together as a 1:32 splitter, a set of 32 phase shifters based on PZTs and
a set of 32 VOAs, realized as MZIs with 2 phase shifters each. The phase shifters of the MZIs
will be based again on PZTs 31

Figure 20: Picture of the twin PCBs that implement a quad-channel driver for PZTs with locapacitance (up to approximately 300 pF) with high output amplitude (>70 Vpp) and high	gh
bandwidth (>10 MHz)	33
Figure 21: Screenshots from the testing of the driver unit of Figure 20. (Left): Output sign with 71.2 Vpp in the case of sinusoidal input at 2.5 MHz. (Right): Output signal with 70 Vpp in the case of a sawtooth input signal at 2.5 MHz).4
Figure 22: Picture of the unit that implements a 32-channel driver for PZTs with hig capacitance (> 1 nF) with high output amplitude (60 Vpp) and moderate bandwidth (10 kHz).	00
Figure 23: Picture of the unit that implements a 160-channel driver for operation of PZ with ultra-high output amplitude (up to 300 Vpp) at quasi-static operation (<1 kHz). The un shown here contains the digital part (RPi micro-computer, the DAC, and the final drivin PCBs each based on the HV257 IC from Microchip, which implements a 32-channel hig	nit ng
voltage sample-and-hold amplifier array	35